

---

# On the Necessity and Effectiveness of Learning the Prior of Variational Auto-Encoder

---

Haowen Xu  
Zhihan Li

Wenxiao Chen  
Youjian Zhao

Jinlin Lai  
Dan Pei

Beijing National Research Center for Information Science and Technology  
Tsinghua University  
Beijing, China

{xhw15, chen-wx17, laijl16, lizhihan17}@mails.tsinghua.edu.cn  
{zhaoyoujian, peidan}@tsinghua.edu.cn

## Abstract

Using powerful posterior distributions is a popular approach to achieving better variational inference. However, recent works showed that the aggregated posterior may fail to match unit Gaussian prior, thus learning the prior becomes an alternative way to improve the lower-bound. In this paper, for the first time in the literature, we prove the necessity and effectiveness of learning the prior when aggregated posterior does not match unit Gaussian prior, analyze why this situation may happen, and propose a hypothesis that learning the prior may improve reconstruction loss, all of which are supported by our extensive experiment results. We show that using learned Real NVP prior and just one latent variable in VAE, we can achieve test NLL comparable to very deep state-of-the-art hierarchical VAE, outperforming many previous works with complex hierarchical VAE architectures.

## 1 Introduction

Variational auto-encoder (VAE) [15, 27] is a powerful deep generative model. The use of *amortized variational inference* makes VAE scalable to deep neural networks and large amount of data. Variational inference demands the intractable true posterior to be approximated by a tractable distribution. The original VAE used factorized Gaussian for both the prior and the variational posterior [15, 27]. Since then, lots of more expressive variational posteriors have been proposed [36, 25, 30, 23, 16, 22, 2]. However, recent work suggested that even with powerful posteriors, VAE may still fail to match *aggregated posterior* to unit Gaussian prior [28], indicating there is still a gap between the approximated and the true posterior.

To improve the lower-bound, one alternative to using powerful posterior distributions is to learn the prior as well, an idea initially suggested by Hoffman and Johnson [11]. Later on, Huang et al. [13] applied Real NVP [7] to learn the prior. Tomczak and Welling [35] proved the optimal prior is the *aggregated posterior*, which they approximate by assembling a mixture of the posteriors with a set of learned pseudo-inputs. Bauer and Mnih [1] constructed a rich prior by multiplying a simple prior with a learned acceptance function. Takahashi et al. [34] introduced the *kernel density trick* to estimate the KL divergence in ELBO and log-likelihood, without explicitly learning the *aggregated posterior*.

Despite the above works, no formal proof has been made to show the necessity and effectiveness of learning the prior. Also, the previous works on prior fail to present comparable results with state-of-the-art VAE models, unless equipped with hierarchical latent variables, making it unclear whether the reported performance gain actually came from the learned prior, or from the complex architecture. In this paper, we will discuss the necessity and effectiveness of learning the prior, and conduct comprehensive experiments on several datasets with learned Real NVP priors and just one latent variable. Our contributions are:

- We are the first to prove the necessity and effectiveness of learning the prior when *aggregated posterior* does not match unit Gaussian prior, give novel analysis on why this situation may happen, and propose novel hypothesis that learning the prior can improve reconstruction loss, all of which are supported by our extensive experiment results.
- We conduct comprehensive experiments on four binarized datasets with four different network architectures. Our results show that VAE with Real NVP prior consistently outperforms standard VAE and Real NVP posterior.
- We are the first to show that using learned Real NVP prior with just one latent variable in VAE, it is possible to achieve test negative log-likelihoods (NLLs) comparable to very deep state-of-the-art hierarchical VAE on these four datasets, outperforming many previous works using complex hierarchical VAE equipped with rich priors/posteriors.
- We demonstrate that the learned prior can avoid assigning high likelihoods to low-quality interpolations on the latent space and to the recently discovered low posterior samples [28].

## 2 Preliminaries

### 2.1 Variational auto-encoder

Variational auto-encoder (VAE) [15, 27] is a deep probabilistic model. It uses a latent variable  $\mathbf{z}$  with prior  $p_\lambda(\mathbf{z})$ , and a conditional distribution  $p_\theta(\mathbf{x}|\mathbf{z})$ , to model the observed variable  $\mathbf{x}$ . The likelihood of a given  $\mathbf{x}$  is formulated as  $p_\theta(\mathbf{x}) = \int_{\mathcal{Z}} p_\theta(\mathbf{x}|\mathbf{z}) p_\lambda(\mathbf{z}) d\mathbf{z}$ , where  $p_\theta(\mathbf{x}|\mathbf{z})$  is typically derived by a neural network with learnable parameter  $\theta$ . Using variational inference, the log-likelihood  $\log p_\theta(\mathbf{x})$  is bounded below by evidence lower-bound (ELBO) of  $\mathbf{x}$  (1):

$$\begin{aligned} \log p_\theta(\mathbf{x}) &\geq \log p_\theta(\mathbf{x}) - D_{KL}[q_\phi(\mathbf{z}|\mathbf{x})||p_\theta(\mathbf{z}|\mathbf{x})] \\ &= \mathbb{E}_{q_\phi(\mathbf{z}|\mathbf{x})} [\log p_\theta(\mathbf{x}|\mathbf{z}) + \log p_\lambda(\mathbf{z}) - \log q_\phi(\mathbf{z}|\mathbf{x})] \\ &= \mathcal{L}(\mathbf{x}; \lambda, \theta, \phi) \\ &= \mathbb{E}_{q_\phi(\mathbf{z}|\mathbf{x})} [\log p_\theta(\mathbf{x}|\mathbf{z})] - D_{KL}[q_\phi(\mathbf{z}|\mathbf{x})||p_\lambda(\mathbf{z})] \end{aligned} \quad (1)$$

$$(2)$$

where  $q_\phi(\mathbf{z}|\mathbf{x})$  is the variational posterior to approximate  $p_\theta(\mathbf{z}|\mathbf{x})$ , derived by a neural network with parameter  $\phi$ . Eq. (2) is one decomposition of (1), where the first term is the *reconstruction loss* of  $\mathbf{x}$ , and the second term is the Kullback Leibler (KL) divergence between  $q_\phi(\mathbf{z}|\mathbf{x})$  and  $p_\lambda(\mathbf{z})$ .

Optimizing  $q_\phi(\mathbf{z}|\mathbf{x})$  and  $p_\theta(\mathbf{x}|\mathbf{z})$  w.r.t. empirical distribution  $p^*(\mathbf{x})$  can be achieved by maximizing “the expected ELBO w.r.t. the empirical distribution  $p^*(\mathbf{x})$ ” (denoted by *elbo* for short hereafter):

$$\mathcal{L}(\lambda, \theta, \phi) = \mathbb{E}_{p^*(\mathbf{x})} [\mathcal{L}(\mathbf{x}; \lambda, \theta, \phi)] = \mathbb{E}_{p^*(\mathbf{x})} \mathbb{E}_{q_\phi(\mathbf{z}|\mathbf{x})} [\log p_\theta(\mathbf{x}|\mathbf{z}) + \log p_\lambda(\mathbf{z}) - \log q_\phi(\mathbf{z}|\mathbf{x})] \quad (3)$$

### 2.2 Real NVP

Real NVP [7] (*RNVP* for short hereafter) is also a deep probabilistic model, and we denote its observed variable by  $\mathbf{z}$  and latent variable by  $\mathbf{w}$ , with marginal distribution  $p_\lambda(\mathbf{z})$  and prior  $p_\xi(\mathbf{w})$ . RNVP relates  $\mathbf{z}$  and  $\mathbf{w}$  by an invertible mapping  $\mathbf{w} = f_\lambda(\mathbf{z})$ , instead of a conditional distribution in VAE. Given the invertibility of  $f_\lambda$ , we have:

$$p_\lambda(\mathbf{z}) = p_\xi(\mathbf{w}) \left| \det \left( \frac{\partial f_\lambda(\mathbf{z})}{\partial \mathbf{z}} \right) \right|, \quad \mathbf{z} = f_\lambda^{-1}(\mathbf{w}) \quad (4)$$

where  $\det(\partial f_\lambda(\mathbf{z})/\partial \mathbf{z})$  is the Jacobian determinant of  $f_\lambda$ . In RNVP,  $f_\lambda$  is composed of  $K$  invertible mappings, where  $f_\lambda(\mathbf{z}) = (f_K \circ \dots \circ f_1)(\mathbf{z})$ , and each  $f_k$  is invertible.  $f_k$  must be carefully designed to ensure that the determinant can be computed efficiently. The original paper of RNVP introduced the *affine coupling layer* as  $f_k$ . Kingma and Dhariwal [17] further introduced *actnorm* and *invertible 1x1 convolution*. Details can be found in their respective papers.

## 3 Learning the prior with RNVP

It is straightforward to obtain a rich prior  $p_\lambda(\mathbf{z})$  from a simple (*i.e.*, with constant parameters) one with RNVP. Denote the simple prior as  $p_\xi(\mathbf{w})$ , while the RNVP mapping as  $\mathbf{w} = f_\lambda(\mathbf{z})$ . We then

obtain Eq. (4) as our prior  $p_\lambda(\mathbf{z})$ . Substitute Eq. (4) into (3), we get to the training objective:

$$\mathcal{L}(\lambda, \theta, \phi) = \mathbb{E}_{p^*(\mathbf{x})} \mathbb{E}_{q_\phi(\mathbf{z}|\mathbf{x})} \left[ \log p_\theta(\mathbf{x}|\mathbf{z}) + \log p_\xi(f_\lambda(\mathbf{z})) + \log \left| \det \left( \frac{\partial f_\lambda(\mathbf{z})}{\partial \mathbf{z}} \right) \right| - \log q_\phi(\mathbf{z}|\mathbf{x}) \right] \quad (5)$$

We mainly use **joint training** [35, 1] (where  $p_\lambda(\mathbf{z})$  is jointly trained along with  $q_\phi(\mathbf{z}|\mathbf{x})$  and  $p_\theta(\mathbf{x}|\mathbf{z})$  by directly maximizing Eq. (5)) in our experiments, but we also consider the other two training strategies: **1) post-hoc training** [1], where  $p_\lambda(\mathbf{z})$  is optimized to match  $q_\phi(\mathbf{z})$  of a standard, pre-trained VAE; and **2) iterative training** (proposed by us), where we alternate *between* training  $p_\theta(\mathbf{x}|\mathbf{z})$  &  $q_\phi(\mathbf{z}|\mathbf{x})$  and training  $p_\lambda(\mathbf{z})$ , for multiple iterations. More details can be found in Appendix B.3.

## 4 The necessity of learning the prior

The *aggregated posterior*, defined as  $q_\phi(\mathbf{z}) = \int_{\mathcal{Z}} q_\phi(\mathbf{z}|\mathbf{x}) p^*(\mathbf{x}) d\mathbf{z}$ , should be equal to  $p_\lambda(\mathbf{z})$ , if VAE is *perfectly trained*, i.e.,  $q_\phi(\mathbf{z}|\mathbf{x}) \equiv p_\theta(\mathbf{z}|\mathbf{x})$  and  $p_\theta(\mathbf{x}) \equiv p^*(\mathbf{x})$  [11]. However, Rosca et al. [28] showed that even with powerful posteriors, the *aggregated posterior* may still not match a unit Gaussian prior, which, we argue, is a practical limitation of neural networks and the existing optimization techniques. To better match the prior and *aggregated posterior*, Hoffman and Johnson [11] suggested a decomposition of *elbo* (Eq. (3)):

$$\mathcal{L}(\lambda, \theta, \phi) = \underbrace{\mathbb{E}_{p^*(\mathbf{x})} \mathbb{E}_{q_\phi(\mathbf{z}|\mathbf{x})} [\log p_\theta(\mathbf{x}|\mathbf{z})]}_{\textcircled{1}} - \underbrace{\text{D}_{KL} [q_\phi(\mathbf{z}) \| p_\lambda(\mathbf{z})]}_{\textcircled{2}} - \underbrace{\mathbb{I}_\phi[Z; X]}_{\textcircled{3}} \quad (6)$$

where  $\textcircled{3}$  is the *mutual information*, defined as  $\mathbb{I}_\phi[Z; X] = \iint q_\phi(\mathbf{z}, \mathbf{x}) \log \frac{q_\phi(\mathbf{z}, \mathbf{x})}{q_\phi(\mathbf{z}) p^*(\mathbf{x})} d\mathbf{z} d\mathbf{x}$ . Since  $p_\lambda(\mathbf{z})$  is only included in  $\textcircled{2}$ , *elbo* can be further enlarged if  $p_\lambda(\mathbf{z})$  is trained to match  $q_\phi(\mathbf{z})$ . However, neither the existence of a better  $p_\lambda(\mathbf{z})$ , nor the necessity of learning the  $p_\lambda(\mathbf{z})$  for reaching the extremum of *elbo*, has been proved under the condition that  $q_\phi(\mathbf{z})$  does not match  $\mathcal{N}(\mathbf{0}, \mathbf{I})$ . In the following, we shall give the proof, and discuss why  $q_\phi(\mathbf{z})$  could not match  $\mathcal{N}(\mathbf{0}, \mathbf{I})$  in practice.

**Proposition 1.** For VAE with flow prior  $p_\lambda(\mathbf{z}) = p_{\mathcal{N}}(f_\lambda(\mathbf{z})) |\det(\partial f_\lambda / \partial \mathbf{z})|$ , where  $p_{\mathcal{N}}(f_\lambda(\mathbf{z})) = \mathcal{N}(\mathbf{0}, \mathbf{I})$ , if  $q_\phi(\mathbf{z}) \neq \mathcal{N}(\mathbf{0}, \mathbf{I})$ , then its training objective (*elbo*):

$$\mathcal{L}(\lambda, \theta, \phi) = \mathbb{E}_{p^*(\mathbf{x})} \mathbb{E}_{q_\phi(\mathbf{z}|\mathbf{x})} \left[ \log p_\theta(\mathbf{x}|\mathbf{z}) + \log p_{\mathcal{N}}(f_\lambda(\mathbf{z})) + \log \left| \det \left( \frac{\partial f_\lambda(\mathbf{z})}{\partial \mathbf{z}} \right) \right| - \log q_\phi(\mathbf{z}|\mathbf{x}) \right]$$

can reach its extremum only if  $f_\lambda \neq f_{\lambda_0}$ , where  $f_{\lambda_0} = \text{id}$  is the identity mapping. Also,  $\forall \theta, \phi$ , if  $q_\phi(\mathbf{z}) \neq \mathcal{N}(\mathbf{0}, \mathbf{I})$ , then there exist  $f_\lambda \neq f_{\lambda_0}$ , s.t.  $\mathcal{L}(\lambda, \theta, \phi) > \mathcal{L}(\lambda_0, \theta, \phi)$ .

*Proof.* See Appendix A.1. □

Since  $\mathcal{L}(\lambda_0, \theta, \phi)$  is exactly the training objective for a standard VAE with unit Gaussian prior, we conclude that when  $q_\phi(\mathbf{z}) \neq \mathcal{N}(\mathbf{0}, \mathbf{I})$ , learning the prior is necessary, and there always exists a  $f_\lambda$  that gives us a higher *elbo* than just using a unit Gaussian prior.

To analyze why  $q_\phi(\mathbf{z})$  does not match the unit Gaussian prior, we start with the following proposition:

**Proposition 2.** Given a finite number of discrete training data, i.e.,  $p^*(\mathbf{x}) = \frac{1}{N} \sum_{i=1}^N \delta(\mathbf{x} - \mathbf{x}^{(i)})$ , if  $p_\theta(\mathbf{x}|\mathbf{z}) = \text{Bernoulli}(\boldsymbol{\mu}_\theta(\mathbf{z}))$ , where the Bernoulli mean  $\boldsymbol{\mu}_\theta(\mathbf{z})$  is produced by the decoder, and  $0 < \mu_\theta^k(\mathbf{z}) < 1$  for each of its  $k$ -th dimensional output, then the optimal decoder  $\boldsymbol{\mu}_\theta(\mathbf{z})$  is:

$$\boldsymbol{\mu}_\theta(\mathbf{z}) = \sum_i w_i(\mathbf{z}) \mathbf{x}^{(i)}, \quad \text{where } w_i(\mathbf{z}) = \frac{q_\phi(\mathbf{z}|\mathbf{x}^{(i)})}{\sum_j q_\phi(\mathbf{z}|\mathbf{x}^{(j)})} \text{ and } \sum_i w_i(\mathbf{z}) = 1 \quad (7)$$

*Proof.* See Appendix A.2. □

Proposition 2 suggests that if  $q_\phi(\mathbf{z}|\mathbf{x})$  for different  $\mathbf{x}$  overlap, then even at the center of  $q_\phi(\mathbf{z}|\mathbf{x}^{(i)})$  of one training point  $\mathbf{x}^{(i)}$ , the optimal decoder will be an *average* of both  $\mathbf{x}^{(i)}$  and other training points  $\mathbf{x}^{(j)}$ , weighted by  $w_i(\mathbf{z})$  and  $w_j(\mathbf{z})$ . However, Rezende and Viola [26] has shown that weighted average like this is likely to cause poor *reconstruction loss* ( $\textcircled{1}$  in Eq. (6)) and “blurry reconstruction”.

Table 1: Average test NLL (lower is better) of different models, with Gaussian prior & Gaussian posterior (“standard”), Gaussian prior & RNVP posterior (“RNVP  $q(z|x)$ ”), and RNVP prior & Gaussian posterior (“RNVP  $p(z)$ ”). The flow depth  $K$  is 20 for RNVP priors and posteriors.

Datasets	DenseVAE			ResnetVAE			PixelVAE		
	standard	RNVP $q(z x)$	RNVP $p(z)$	standard	RNVP $q(z x)$	RNVP $p(z)$	standard	RNVP $q(z x)$	RNVP $p(z)$
StaticMNIST	88.84	86.07	<b>84.87</b>	82.95	80.97	<b>79.99</b>	79.47	79.09	<b>78.92</b>
MNIST	84.48	82.53	<b>80.43</b>	81.07	79.53	<b>78.58</b>	78.64	78.41	<b>78.15</b>
FashionMNIST	228.60	227.79	<b>226.11</b>	226.17	225.02	<b>224.09</b>	224.22	223.81	<b>223.40</b>
Omniglot	106.42	102.97	<b>102.19</b>	96.99	94.30	<b>93.61</b>	89.83	89.69	<b>89.61</b>

Table 2: Average test NLL of ResnetVAE + RNVP prior with different flow depth  $K$

Datasets	Flow depth $K$ for RNVP prior							
	0	1	2	5	10	20	30	50
StaticMNIST	82.95	81.76	81.30	80.64	80.26	79.99	79.90	<b>79.84</b>
MNIST	81.07	80.02	79.58	79.09	78.75	78.58	78.52	<b>78.49</b>
FashionMNIST	226.17	225.27	224.78	224.37	224.18	224.09	<b>224.07</b>	<b>224.07</b>
Omniglot	96.99	96.20	95.35	94.47	93.92	93.61	93.53	<b>93.52</b>

One direction to optimize Eq. (6) is to enlarge ①, and to achieve this, it is a crucial goal to reduce the weight  $w_j(\mathbf{z})$ ,  $j \neq i$  for  $\mathbf{z}$  near the center of every  $q_\phi(\mathbf{z}|\mathbf{x}^{(i)})$ .

In order to achieve this goal for Gaussian posterior, one way is to reduce the standard deviations (std) of  $q_\phi(\mathbf{z}|\mathbf{x})$  for all  $\mathbf{x}$ . But smaller stds for all  $\mathbf{x}$  is likely to cause *aggregated posterior*  $q_\phi(\mathbf{z})$  to become more dissimilar with unit Gaussian prior, *i.e.*, enlarging ② in Eq. (6). Also, there is trade-off between *reconstruction loss* and *mutual information*, see Appendix A.3. From above analysis, we can see that, at least for Gaussian posterior, **there is a trade-off between ① and (② + ③) in Eq. (6). Due to this trade-off, ② is extremely hard to be optimal (*i.e.*,  $q_\phi(\mathbf{z}) \equiv p_\lambda(\mathbf{z})$ ). We think this is one important reason why  $q_\phi(\mathbf{z})$  cannot match  $p_\lambda(\mathbf{z})$  in practice.**

$p_\lambda(\mathbf{z})$  appears only in ②. With learned prior, the influence of ② on the training objective (Eq. (6)) is much smaller, thus the trade-off seems to occur mainly between ① and ③. Since the numerical values of ① is typically much larger than ③ in practice, the new trade-off is likely to cause ① to increase. Thus, we propose the hypothesis that a learned prior may improve *reconstruction loss*.

Although learning the prior can reduce ②, a learned prior does not necessarily make KL divergence smaller (as opposed to what was previously implied by Bauer and Mnih [1]), since the KL divergence  $\mathbb{E}_{p^*(\mathbf{x})} D_{KL}[q_\phi(\mathbf{z}|\mathbf{x})||p_\lambda(\mathbf{z})] = ② + ③$  is also affected by the *mutual information* (③).

Rezende and Viola [26] has proved when  $p_\theta(\mathbf{x}|\mathbf{z}) = \mathcal{N}(\boldsymbol{\mu}_\theta(\mathbf{z}), \sigma^2 \mathbf{I})$ , where  $\sigma$  is a fixed constant, the optimal decoder is also  $\boldsymbol{\mu}_\theta(\mathbf{z}) = \sum_i w_i(\mathbf{z}) \mathbf{x}^{(i)}$ , thus our analysis naturally holds in such situation.

For non-Gaussian posteriors, as long as  $q_\phi(\mathbf{z}|\mathbf{x})$  is defined on the whole  $\mathbb{R}^n$  (*e.g.*, flow posteriors derived by applying continuous mappings on  $\mathcal{N}(\mathbf{0}, \mathbf{I})$ ), it is possible that  $w_j(\mathbf{z})$  for  $\mathbf{z}$  near the center of  $q_\phi(\mathbf{z}|\mathbf{x}^{(i)})$  is not small enough, causing “blurry reconstruction”. Learning the prior may help optimize such posteriors to produce a better  $w_j(\mathbf{z})$ . We also suspect this problem may occur with other element-wise  $p_\theta(\mathbf{x}|\mathbf{z})$ . These concerns highlight the necessity of learning the prior.

## 5 Experiments

### 5.1 Setup

**Datasets** We use four datasets in our experiments: statically and dynamically binarized MNIST [19, 29], FashionMNIST [37] and Omniglot [18]. Details of these datasets can be found in Appendix B.1.

**Models** We perform systematically controlled experiments, using the following VAE variants: (1) **DenseVAE**, whose encoder and decoder are composed of dense layers; (2) **ConvVAE**, with

Table 3: Average test NLL of ResnetVAE, with RNVP posterior (“RNVP  $q(z|x)$ ”), RNVP prior (“RNVP  $p(z)$ ”), and both RNVP prior & posterior (“both”). Flow depth  $K = 20$ .

Datasets	ResnetVAE		
	RNVP $q(z x)$	RNVP $p(z)$	both
StaticMNIST	80.97	79.99	<b>79.87</b>
MNIST	79.53	78.58	<b>78.56</b>
FashionMNIST	225.02	224.09	<b>224.08</b>
Omniglot	94.30	<b>93.61</b>	93.68

Table 5: Test NLL on StaticMNIST. “ $\dagger$ ” indicates a hierarchical model with 2 latent variables, while “ $\ddagger$ ” indicates at least 3 latent variables.

Model	NLL
<i>Models without PixelCNN decoder</i>	
ConvHVAE + Lars prior $^\dagger$ [1]	81.70
ConvHVAE + VampPrior $^\dagger$ [35]	81.09
VAE + IAF $^\ddagger$ [16]	79.88
BIVA $^\ddagger$ [20]	<b>78.59</b>
<i>Our ConvVAE + RNVP <math>p(z)</math>, <math>K = 50</math></i>	80.09
<i>Our ResnetVAE + RNVP <math>p(z)</math>, <math>K = 50</math></i>	79.84
<i>Models with PixelCNN decoder</i>	
VLAE $^\ddagger$ [5]	79.03
PixelHVAE + VampPrior $^\dagger$ [35]	79.78
<i>Our PixelVAE + RNVP <math>p(z)</math>, <math>K = 50</math></i>	<b>79.01</b>

Table 4: Average test NLL of ResnetVAE, with prior trained by: *joint* training, *iterative* training, *post-hoc* training, and standard VAE (“none”) as reference. Flow depth  $K = 20$ .

Datasets	ResnetVAE			
	joint	iterative	post-hoc	none
StaticMNIST	<b>79.99</b>	80.63	80.86	82.95
MNIST	<b>78.58</b>	79.61	79.90	81.07
FashionMNIST	<b>224.09</b>	224.88	225.22	226.17
Omniglot	<b>93.61</b>	94.43	94.87	96.99

Table 6: Test NLL on MNIST. “ $\dagger$ ” and “ $\ddagger$ ” has the same meaning as Table 5.

Model	NLL
<i>Models without PixelCNN decoder</i>	
ConvHVAE + Lars prior $^\dagger$ [1]	80.30
ConvHVAE + VampPrior $^\dagger$ [35]	79.75
VAE + IAF $^\ddagger$ [16]	79.10
BIVA $^\ddagger$ [20]	<b>78.41</b>
<i>Our ConvVAE + RNVP <math>p(z)</math>, <math>K = 50</math></i>	78.61
<i>Our ResnetVAE + RNVP <math>p(z)</math>, <math>K = 50</math></i>	78.49
<i>Models with PixelCNN decoder</i>	
VLAE $^\ddagger$ [5]	78.53
PixelVAE $^\dagger$ [10]	79.02
PixelHVAE + VampPrior $^\dagger$ [35]	78.45
<i>Our PixelVAE + RNVP <math>p(z)</math>, <math>K = 50</math></i>	<b>78.12</b>

convolutional layers; (3) **ResnetVAE**, with ResNet layers [38]; and (4) **PixelVAE** [10], with several PixelCNN layers on top of the ResnetVAE decoder. For RNVP priors and posteriors, we use  $K$  blocks of invertible mappings ( $K$  is called *flow depth* hereafter), while each block contains an *invertible dense*, a *dense coupling layer*, and an *actnorm* [7, 17]. More details can be found in Appendix B.2.

**Training and evaluation** Unless specified, all experiments are repeated for 3 times, and the metric means are reported. We use Adam [14] and adopt warm up (KL annealing) [3] to train all models. We perform early-stopping using negative log-likelihood (NLL) on validation set, to prevent over-fitting on StaticMNIST and on all datasets with PixelVAE. For evaluation, we use 1,000 samples to estimate NLL and other metrics on test set, unless specified. More details can be found in Appendix B.3.

## 5.2 Quantitative results

Table 1 shows the NLLs of DenseVAE, ResnetVAE and PixelVAE with flow depth  $K = 20$ , where larger  $K$  are not thoroughly tested due to limited computational resources. ConvVAE can be found in Table B.3 in the Appendix, which has similar trends as ResnetVAE; the standard deviations can also be found in the Appendix. We can see that RNVP prior consistently outperforms standard VAE and RNVP posterior in test NLL, with as large improvement as about 2 nats on ResnetVAE, and even larger improvement on DenseVAE. The improvement is not so significant on PixelVAE, which is not surprising because PixelVAE encodes less information in the latent variable [10].

Table 2 shows the NLLs of ResnetVAE with different flow depth  $K$ . Even  $K = 1$ , RNVP prior can improve NLLs by about 1 nat. There is no over-fitting for  $K$  up to 50. However, we do not claim learning the prior will not cause over-fitting; this only suggests RNVP prior does not over-fit easily.

Table 3 shows that using both RNVP prior and posterior shows no significant advantage over using RNVP prior only. This, in conjunction with the results of RNVP prior and posterior from Table 1, highlights that learning the prior is crucial for good NLLs, supporting our statements in Proposition 1.

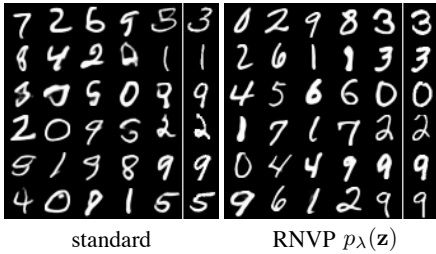


Figure 1: Sample means from  $p_\lambda(\mathbf{z})$  of ResnetVAE with: (left) unit Gaussian prior; (right) RNVP prior. The last column of each 6x6 grid show the images from the training set, most similar to the second-to-last column in pixel-wise L2 distance.

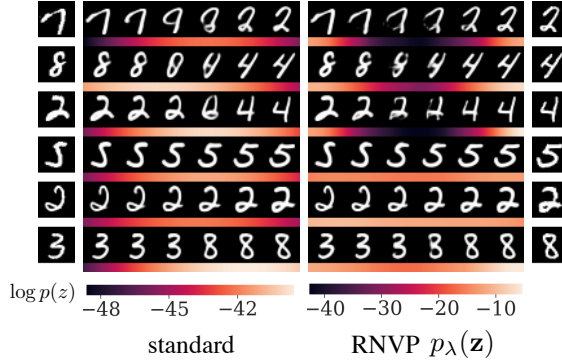


Figure 2: Interpolations of  $\mathbf{z}$  from ResnetVAE, between the centers of  $q_\phi(\mathbf{z}|\mathbf{x})$  of two training points, and heatmaps of  $\log p_\lambda(\mathbf{z})$ . The left-most and right-most columns are the original training points.

Table 7: Average test *elbo*, *reconstruction loss* (“*recons*”),  $\mathbb{E}_{p^*(\mathbf{x})} D_{KL}[q_\phi(\mathbf{z}|\mathbf{x}) \| p_\lambda(\mathbf{z})]$  (“*kl*”), and  $\mathbb{E}_{p^*(\mathbf{x})} D_{KL}[q_\phi(\mathbf{z}|\mathbf{x}) \| p_\theta(\mathbf{z}|\mathbf{x})]$  (“*kl<sub>z|x</sub>*”) of ResnetVAE with different priors.

Datasets	standard				RNVP $p(z)$			
	<i>lb</i>	<i>recons</i>	<i>kl</i>	<i>kl<sub>z x</sub></i>	<i>lb</i>	<i>recons</i>	<i>kl</i>	<i>kl<sub>z x</sub></i>
StaticMNIST	-87.61	-60.09	<b>27.52</b>	4.67	<b>-82.85</b>	<b>-54.32</b>	28.54	<b>2.87</b>
MNIST	-84.62	-58.70	<b>25.92</b>	3.55	<b>-80.34</b>	<b>-53.64</b>	26.70	<b>1.76</b>
FashionMNIST	-228.91	-208.94	<b>19.96</b>	2.74	<b>-225.97</b>	<b>-204.66</b>	21.31	<b>1.88</b>
Omniglot	-104.87	-66.98	<b>37.89</b>	7.88	<b>-99.60</b>	<b>-61.21</b>	38.39	<b>5.99</b>

Table 4 shows the NLLs of *iterative training* and *post-hoc training* with ResnetVAE. Although still not comparable to *joint training*, both methods can bring large improvement in NLLs over standard VAE. Also, *iterative training* even further outperforms *post-hoc training* by a large margin.

In Tables 5 and 6, we compare ResnetVAE and PixelVAE with RNVP prior to other approaches on StaticMNIST and MNIST. The results on Omniglot and FashionMNIST have a similar trend, and can be found in Tables B.8 and B.9. All models except ours used at least 2 latent variables. Our ResnetVAE with RNVP prior,  $K = 50$  is second only to BIVA among all models without PixelCNN decoder, and ranks the first among all models with PixelCNN decoder. On MNIST, the NLL of our model is very close to BIVA, while the latter used 6 latent variables and very complicated architecture. Although BIVA has a much lower NLL on StaticMNIST, in contrast to our paper, the BIVA paper [20] did not report using validation data for early-stopping, indicating the gap should mainly be attributed to having fewer training data. Meanwhile, our ConvVAE with RNVP prior,  $K = 50$  has lower test NLL than ConvHVAE with *Lars prior* and *VampPrior*. Since ConvVAE is undoubtedly a simpler architecture than ConvHVAE (which has 2 latent variables), it is likely that our improvement comes from the RNVP prior rather than the different architecture. **Tables 5 and 6 show that using RNVP prior with just one latent variable, it is possible to achieve NLLs comparable to very deep state-of-the-art VAE (BIVA), outperforming many previous works (including works on priors, and works of complicated hierarchical VAE equipped with rich posteriors like VAE + IAF). This discovery shows that simple VAE architectures with learned prior and a small number of latent variables is a promising direction.**

### 5.3 Qualitative results

Fig. 1 samples images from ResnetVAE trained with different methods. Compared to standard ResnetVAE, ResnetVAE with RNVP prior produces fewer digits that are hard to interpret. The last column of each 6x6 grid show the images from the training set, most similar to the second-to-last column in pixel-wise L2 distance. However, there are differences between the last two columns, indicating our model is not just memorizing the training data. More samples are in Appendix B.7.

Table 8: Avg. number of *active units* of ResnetVAE with different priors.

Datasets	ResnetVAE	
	standard	RNVP $p(z)$
StaticMNIST	30	<b>40</b>
MNIST	25.3	<b>40</b>
FashionMNIST	27	<b>64</b>
Omniglot	59.3	<b>64</b>

Table 9: Avg. *reconstruction loss*,  $\mathbb{E}_{p^*(\mathbf{x})} D_{KL}[q_\phi(\mathbf{z}|\mathbf{x})||p_\lambda(\mathbf{z})]$  (“*kl*”) and *active units* (“*au*”) of ResnetVAE with *iteratively trained* and *post-hoc trained* RNVP priors.

Datasets	iterative			post-hoc		
	<i>recons</i>	<i>kl</i>	<i>au</i>	<i>recons</i>	<i>kl</i>	<i>au</i>
StaticMNIST	<b>-58.0</b>	26.4	<b>38.7</b>	-60.1	<b>25.3</b>	30
DynamicMNIST	<b>-57.2</b>	25.1	<b>40</b>	-58.7	<b>24.7</b>	25.3
FashionMNIST	<b>-207.8</b>	19.4	<b>64</b>	-208.9	<b>19.0</b>	27
Omniglot	<b>-63.3</b>	37.9	<b>64</b>	-67.0	<b>35.8</b>	59.3

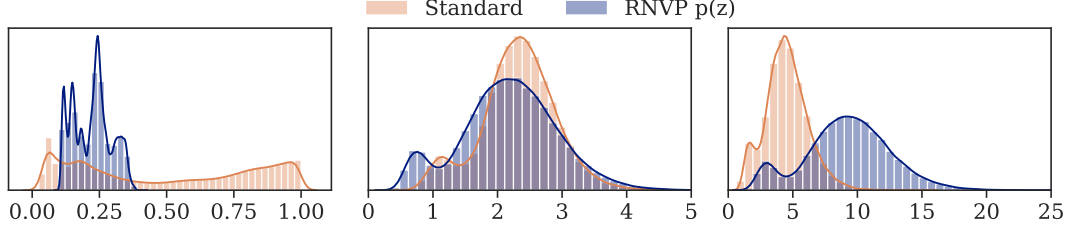


Figure 3: Histograms of: (left) per-dimensional stds of  $q_\phi(\mathbf{z}|\mathbf{x})$ ; (middle) distances between closest pairs of  $q_\phi(\mathbf{z}|\mathbf{x})$ ; and (right) *normalized distances*. See Appendix B.4 for formulation.

#### 5.4 Improved reconstruction loss and other experimental results with learned prior

In this section, we will show the improved reconstruction loss and other experimental results with learned RNVP prior, which supports Proposition 2.

**Better reconstruction loss, but larger KL divergence** In Table 7, *elbo* and *reconstruction loss* ( $\mathbb{E}_{p^*(\mathbf{x})} \mathbb{E}_{q_\phi(\mathbf{z}|\mathbf{x})} [\log p_\theta(\mathbf{x}|\mathbf{z})]$ ) of ResnetVAE with RNVP prior are substantially higher than standard ResnetVAE, just as the trend of test log-likelihood (LL) in Table 1. Metrics of other models are in Tables B.11 to B.14.

On the contrary,  $\mathbb{E}_{p^*(\mathbf{x})} D_{KL}[q_\phi(\mathbf{z}|\mathbf{x})||p_\lambda(\mathbf{z})]$  are larger, while  $\mathbb{E}_{p^*(\mathbf{x})} D_{KL}[q_\phi(\mathbf{z}|\mathbf{x})||p_\theta(\mathbf{z}|\mathbf{x})]$  are smaller. Since  $q_\phi(\mathbf{z}) = \int q_\phi(\mathbf{z}|\mathbf{x}) p^*(\mathbf{x}) d\mathbf{x}$  and  $p_\lambda(\mathbf{z}) = \int p_\theta(\mathbf{x}|\mathbf{z}) p_\theta(\mathbf{x}) d\mathbf{x}$ , the fact that RNVP prior has both better test LL (*i.e.*,  $p_\theta(\mathbf{x})$  is closer to  $p^*(\mathbf{x})$ ) and lower  $\mathbb{E}_{p^*(\mathbf{x})} D_{KL}[q_\phi(\mathbf{z}|\mathbf{x})||p_\theta(\mathbf{z}|\mathbf{x})]$  should suggest  $q_\phi(\mathbf{z})$  is closer to  $p_\lambda(\mathbf{z})$ , hence lower  $D_{KL}[q_\phi(\mathbf{z})||p_\lambda(\mathbf{z})]$ . And since  $\mathbb{E}_{p^*(\mathbf{x})} D_{KL}[q_\phi(\mathbf{z}|\mathbf{x})||p_\lambda(\mathbf{z})] = D_{KL}[q_\phi(\mathbf{z})||p_\lambda(\mathbf{z})] + \mathbb{I}_\phi[Z; X]$  (Eq. (6)), this should suggest a larger  $\mathbb{I}_\phi[Z; X]$ , *i.e.*, *mutual information*. All these facts are consistent with our analysis based on Proposition 2. Note that, under suitable conditions, *reconstruction loss* and  $\mathbb{E}_{p^*(\mathbf{x})} D_{KL}[q_\phi(\mathbf{z}|\mathbf{x})||p_\lambda(\mathbf{z})]$  can happen to be both smaller (*e.g.*, the results of DenseVAE on StaticMNIST in Table B.11).

**Smaller standard deviation of Gaussian posterior with RNVP prior** In Fig. 3, we plot the histograms of per-dimensional stds of  $q_\phi(\mathbf{z}|\mathbf{x})$ , as well as the distances and *normalized distances* (which is roughly distance/std) between each closest pair of  $q_\phi(\mathbf{z}|\mathbf{x})$ . Detailed formulations can be found in Appendix B.4. The std of RNVP prior are substantially smaller, while the *normalized distances* are larger. Larger *normalized distances* indicate less density of  $q_\phi(\mathbf{z}|\mathbf{x})$  to be overlapping, hence better *reconstruction loss* according to Eq. (7). This fact is a direct evidence of Proposition 2.

**More active units** Table 8 counts the *active units* [4] of ResnetVAE with different priors, which quantifies the number of latent dimensions used for encoding information from input data. RNVP prior can cause all units to be active, which is in sharp contrast to standard VAE. It has long been a problem of VAE that the number of *active units* is small, often attributed to the over-regularization of the unit Gaussian prior [11, 35]. Learning the prior can be an effective cure for this problem.

**Iterative training can lead to increased active units and improved reconstruction loss** Table 9 shows that, compared to *post-hoc training*, *iterative training* can lead to increased number of *active*

units and larger *reconstruction loss*, but larger  $\mathbb{E}_{p^*(\mathbf{x})} D_{KL}[q_\phi(\mathbf{z}|\mathbf{x})||p_\lambda(\mathbf{z})]$ . Proposition 2 suggests that a larger *reconstruction loss* can only be obtained with improved  $p_\lambda(\mathbf{z})$ . However, the prior is in turn determined by  $q_\phi(\mathbf{z}|\mathbf{x})$  and  $p_\theta(\mathbf{x}|\mathbf{z})$  according to Eq. (6). Thus, it is important to alternate *between training  $p_\theta(\mathbf{x}|\mathbf{z})$  &  $q_\phi(\mathbf{z}|\mathbf{x})$  and training  $p_\lambda(\mathbf{z})$* . This is why *iterative training* can result in larger *reconstruction loss* than *post-hoc training*.

### 5.5 Learned prior on interpolated $\mathbf{z}$ and low posterior samples

The standard deviations of  $q_\phi(\mathbf{z}|\mathbf{x})$  are not reduced equally. Instead, they are reduced according to the dissimilarity between neighbors. This can result in a fruitful  $p_\lambda(\mathbf{z})$ , learned to score the interpolations of  $\mathbf{z}$  between the centers of  $q_\phi(\mathbf{z}|\mathbf{x}^{(i)})$  and  $q_\phi(\mathbf{z}|\mathbf{x}^{(j)})$  of two training points  $\mathbf{x}^{(i)}$  and  $\mathbf{x}^{(j)}$ . See Fig. 2. RNVP prior learns to give low likelihoods to hard-to-interpret interpolated samples (the first three rows), in contrast to unit Gaussian prior. However, for good quality interpolations (the last three rows), RNVP prior grants high likelihoods. In contrast, the unit Gaussian prior assigns high likelihoods to all interpolations, even when the samples are hard to interpret.

Rosca et al. [28] observed that part of the samples from unit Gaussian prior can have low  $q_\phi(\mathbf{z})$  and low visual quality, and they name these samples the “*low posterior samples*”. Unlike this paper, they tried various approaches to match  $q_\phi(\mathbf{z})$  to unit Gaussian  $p_\lambda(\mathbf{z})$ , including adversarial training methods, but still found *low posterior samples* scattering across the whole prior. Learning the prior can avoid having high  $p_\lambda(\mathbf{z})$  on low posterior samples (see Appendix B.9). Since we have analyzed why  $q_\phi(\mathbf{z})$  cannot match  $p_\lambda(\mathbf{z})$ , we suggest to adopt learned prior as a cheap solution to this problem.

## 6 Related work

Learned priors, as a natural choice for the conditional priors of intermediate variables, have long been unintentionally used in hierarchical VAEs [27, 32, 16, 20]. A few works were proposed to enrich the priors of VAE, *e.g.*, Gaussian mixture priors [23, 6], Bayesian non-parametric priors [24, 9], and auto-regressive priors [10, 5], without the awareness of its relationship with the *aggregated posterior*, until the analysis made by Hoffman and Johnson [11]. Since then, several attempts have been made in matching the prior to *aggregated posterior*, by using Real NVP [13], variational mixture of posteriors [35], learned accept/reject sampling [1], and kernel density trick [34]. However, none of these works proved the necessity of learning the prior, nor did they recognize the improved reconstruction loss induced by learned prior. Furthermore, they did not show that learned prior with just one latent variable can achieve comparable results to those of many deep hierarchical VAEs.

The trade-off between reconstruction loss and KL divergence was also discussed by Rezende and Viola [26], but instead of relieving the resistance from the prior, they proposed to convert the reconstruction loss into an optimization constraint, so as to trade for better reconstruction at the cost of larger KL (and ELBO). Meanwhile, Rosca et al. [28] demonstrated failed attempts in matching *aggregated posterior* to a fixed prior with expressive posteriors, and observed *low posterior samples* problem. We provide analysis on why their attempts failed, prove the necessity of learning the prior, and show the *low posterior samples* can also be avoided by learned prior.

## 7 Conclusion

In this paper, for the first time in the literature, we proved the necessity and effectiveness of learning the prior in VAE when aggregated posterior does not match unit Gaussian prior, analyzed why this situation may happen, and proposed a hypothesis that learning the prior may improve reconstruction loss, all of which are supported by our extensive experiment results. Using learned Real NVP prior with just one latent variable in VAE, we managed to achieve test NLLs comparable to very deep state-of-the-art hierarchical VAE, outperforming many previous works of complex hierarchical VAEs equipped with rich priors/posteriors. Furthermore, we demonstrated that the learned prior can avoid assigning high likelihoods to low-quality interpolations on the latent space and to the recently discovered low posterior samples.

We believe this paper is an important step towards simple VAE architectures with learned prior and a small number of latent variables, which potentially can be more scalable to large datasets than those complex VAE architectures.



## References

- [1] Matthias Bauer and Andriy Mnih. “Resampled Priors for Variational Autoencoders”. In: *arXiv preprint arXiv:1810.11428* (2018).
- [2] Rianne van den Berg, Leonard Hasenclever, Jakub M. Tomczak, and Max Welling. “Sylvester Normalizing Flows for Variational Inference”. In: *arXiv:1803.05649 [cs, stat]* (Mar. 2018).
- [3] Samuel Bowman, Luke Vilnis, Oriol Vinyals, Andrew M. Dai, Rafal Jozefowicz, and Samy Bengio. “Generating Sentences from a Continuous Space.” In: *Proceedings of the Twentieth Conference on Computational Natural Language Learning (CoNLL)*. 2016.
- [4] Yuri Burda, Roger Grosse, and Ruslan Salakhutdinov. “Importance Weighted Autoencoders”. In: *arXiv preprint arXiv:1509.00519* (2015).
- [5] Xi Chen, Diederik P. Kingma, Tim Salimans, Yan Duan, Prafulla Dhariwal, John Schulman, Ilya Sutskever, and Pieter Abbeel. “Variational Lossy Autoencoder”. In: *5th International Conference on Learning Representations, ICLR 2017, Toulon, France, April 24-26, 2017, Conference Track Proceedings*. 2017.
- [6] Nat Dilokthanakul, Pedro AM Mediano, Marta Garnelo, Matthew CH Lee, Hugh Salimbeni, Kai Arulkumaran, and Murray Shanahan. “Deep Unsupervised Clustering with Gaussian Mixture Variational Autoencoders”. In: *arXiv preprint arXiv:1611.02648* (2016).
- [7] Laurent Dinh, Jascha Sohl-Dickstein, and Samy Bengio. “Density Estimation Using Real NVP”. In: *arXiv:1605.08803 [cs, stat]* (May 2016).
- [8] Izrail Moiseevitch Gelfand and Richard A. Silverman. *Calculus of Variations*. Courier Corporation, 2000.
- [9] Prasoon Goyal, Zhiting Hu, Xiaodan Liang, Chenyu Wang, and Eric P. Xing. “Nonparametric Variational Auto-Encoders for Hierarchical Representation Learning”. In: *Proceedings of the IEEE International Conference on Computer Vision*. 2017, pp. 5094–5102.
- [10] Ishaan Gulrajani, Kundan Kumar, Faruk Ahmed, Adrien Ali Taïga, Francesco Visin, David Vázquez, and Aaron C. Courville. “PixelVAE: A Latent Variable Model for Natural Images”. In: *5th International Conference on Learning Representations, ICLR 2017, Toulon, France, April 24-26, 2017, Conference Track Proceedings*. 2017.
- [11] Matthew D. Hoffman and Matthew J. Johnson. “Elbo Surgery: Yet Another Way to Carve up the Variational Evidence Lower Bound”. In: *Workshop in Advances in Approximate Bayesian Inference, NIPS*. 2016.
- [12] Kurt Hornik. “Approximation Capabilities of Multilayer Feedforward Networks”. In: *Neural networks* 4.2 (1991), pp. 251–257.
- [13] Chin-Wei Huang, Ahmed Touati, Laurent Dinh, Michal Drozdal, Mohammad Havaei, Laurent Charlin, and Aaron Courville. “Learnable Explicit Density for Continuous Latent Space and Variational Inference”. In: *arXiv:1710.02248 [cs, stat]* (Oct. 2017).
- [14] Diederik P. Kingma and Jimmy Ba. “Adam: A Method for Stochastic Optimization”. In: *3rd International Conference on Learning Representations, ICLR 2015, San Diego, CA, USA, May 7-9, 2015, Conference Track Proceedings*. 2015.
- [15] Diederik P Kingma and Max Welling. “Auto-Encoding Variational Bayes”. In: *Proceedings of the International Conference on Learning Representations*. 2014.
- [16] Diederik P. Kingma, Tim Salimans, Rafal Jozefowicz, Xi Chen, Ilya Sutskever, and Max Welling. “Improved Variational Inference with Inverse Autoregressive Flow”. In: *Advances in Neural Information Processing Systems*. 2016, pp. 4743–4751.
- [17] Durk P Kingma and Prafulla Dhariwal. “Glow: Generative Flow with Invertible 1x1 Convolutions”. In: *Advances in Neural Information Processing Systems 31*. Ed. by S. Bengio, H. Wallach, H. Larochelle, K. Grauman, N. Cesa-Bianchi, and R. Garnett. Curran Associates, Inc., 2018, pp. 10215–10224.
- [18] B. M. Lake, R. Salakhutdinov, and J. B. Tenenbaum. “Human-Level Concept Learning through Probabilistic Program Induction”. en. In: *Science* 350.6266 (Dec. 2015), pp. 1332–1338. ISSN: 0036-8075, 1095-9203. DOI: 10.1126/science.aab3050.
- [19] Hugo Larochelle and Iain Murray. “The Neural Autoregressive Distribution Estimator”. In: *Proceedings of the Fourteenth International Conference on Artificial Intelligence and Statistics*. 2011, pp. 29–37.

- [20] Lars Maaløe, Marco Fraccaro, Valentin Liévin, and Ole Winther. “BIVA: A Very Deep Hierarchy of Latent Variables for Generative Modeling”. In: *arXiv:1902.02102 [cs, stat]* (Feb. 2019).
- [21] Andrew L. Maas, Awni Y. Hannun, and Andrew Y. Ng. “Rectifier Nonlinearities Improve Neural Network Acoustic Models”. In: *Proc. Icml*. Vol. 30. 2013, p. 3.
- [22] Lars Mescheder, Sebastian Nowozin, and Andreas Geiger. “Adversarial Variational Bayes: Unifying Variational Autoencoders and Generative Adversarial Networks”. In: *Proceedings of the 34th International Conference on Machine Learning-Volume 70*. JMLR. org, 2017, pp. 2391–2400.
- [23] Eric Nalisnick, Lars Hertel, and Padhraic Smyth. “Approximate Inference for Deep Latent Gaussian Mixtures”. In: *NIPS Workshop on Bayesian Deep Learning*. Vol. 2. 2016.
- [24] Eric T. Nalisnick and Padhraic Smyth. “Stick-Breaking Variational Autoencoders”. In: *5th International Conference on Learning Representations, ICLR 2017, Toulon, France, April 24-26, 2017, Conference Track Proceedings*. 2017.
- [25] Danilo Rezende and Shakir Mohamed. “Variational Inference with Normalizing Flows”. In: *Proceedings of the 32nd International Conference on Machine Learning (ICML-15)*. 2015, pp. 1530–1538.
- [26] Danilo Jimenez Rezende and Fabio Viola. “Taming VAEs”. en. In: *arXiv:1810.00597 [cs, stat]* (Oct. 2018).
- [27] Danilo Jimenez Rezende, Shakir Mohamed, and Daan Wierstra. “Stochastic Backpropagation and Approximate Inference in Deep Generative Models”. In: *Proceedings of the 31st International Conference on Machine Learning - Volume 32*. ICML’14. Beijing, China: JMLR.org, 2014, pp. II–1278–II–1286.
- [28] Mihaela Rosca, Balaji Lakshminarayanan, and Shakir Mohamed. “Distribution Matching in Variational Inference”. In: *arXiv preprint arXiv:1802.06847* (2018).
- [29] Ruslan Salakhutdinov and Iain Murray. “On the Quantitative Analysis of Deep Belief Networks”. In: *Proceedings of the 25th International Conference on Machine Learning*. ACM, 2008, pp. 872–879.
- [30] Tim Salimans, Diederik Kingma, and Max Welling. “Markov Chain Monte Carlo and Variational Inference: Bridging the Gap”. In: *Proceedings of the 32nd International Conference on Machine Learning (ICML-15)*. 2015, pp. 1218–1226.
- [31] Tim Salimans, Andrej Karpathy, Xi Chen, and Diederik P. Kingma. “PixelCNN++: Improving the PixelCNN with Discretized Logistic Mixture Likelihood and Other Modifications”. In: *5th International Conference on Learning Representations, ICLR 2017, Toulon, France, April 24-26, 2017, Conference Track Proceedings*. 2017.
- [32] Casper Kaae Sønderby, Tapani Raiko, Lars Maaløe, Søren Kaae Sønderby, and Ole Winther. “Ladder Variational Autoencoders”. In: *Advances in Neural Information Processing Systems*. 2016, pp. 3738–3746.
- [33] Masashi Sugiyama, Taiji Suzuki, and Takafumi Kanamori. *Density Ratio Estimation in Machine Learning*. Cambridge University Press, 2012.
- [34] Hiroshi Takahashi, Tomoharu Iwata, Yuki Yamanaka, Masanori Yamada, and Satoshi Yagi. “Variational Autoencoder with Implicit Optimal Priors”. In: *arXiv:1809.05284 [cs, stat]* (Sept. 2018).
- [35] Jakub Tomczak and Max Welling. “VAE with a VampPrior”. In: *International Conference on Artificial Intelligence and Statistics*. 2018, pp. 1214–1223.
- [36] Dustin Tran, Rajesh Ranganath, and David M. Blei. “Variational Gaussian Process”. In: *4th International Conference on Learning Representations, ICLR 2016, San Juan, Puerto Rico, May 2-4, 2016, Conference Track Proceedings*. 2016.
- [37] Han Xiao, Kashif Rasul, and Roland Vollgraf. “Fashion-MNIST: A Novel Image Dataset for Benchmarking Machine Learning Algorithms”. In: *arXiv:1708.07747 [cs, stat]* (Aug. 2017).
- [38] Sergey Zagoruyko and Nikos Komodakis. “Wide Residual Networks”. In: *arXiv preprint arXiv:1605.07146* (2016).

## A Proof details

### A.1 Proof for Proposition 1

The training objective for VAE with flow prior  $p_\lambda(\mathbf{z}) = p_{\mathcal{N}}(f_\lambda(\mathbf{z})) |\det(\partial f_\lambda / \partial \mathbf{z})|$  is:

$$\mathcal{L}(\lambda, \theta, \phi) = \mathbb{E}_{p^*(\mathbf{x})} \mathbb{E}_{q_\phi(\mathbf{z}|\mathbf{x})} \left[ \log p_\theta(\mathbf{x}|\mathbf{z}) - \log q_\phi(\mathbf{z}|\mathbf{x}) + \log \left| \det \left( \frac{\partial f_\lambda}{\partial \mathbf{z}} \right) \right| + \log p_{\mathcal{N}}(f_\lambda(\mathbf{z})) \right]$$

where  $p_{\mathcal{N}}(\cdot)$  denotes unit Gaussian distribution  $\mathcal{N}(\mathbf{0}, \mathbf{I})$ . Meanwhile, the training objective of a standard VAE with prior  $p_{\mathcal{N}}(\mathbf{z})$  is:

$$\mathcal{L}_{\text{VAE}}(\theta, \phi) = \mathbb{E}_{p^*(\mathbf{x})} \mathbb{E}_{q_\phi(\mathbf{z}|\mathbf{x})} [\log p_\theta(\mathbf{x}|\mathbf{z}) - \log q_\phi(\mathbf{z}|\mathbf{x}) + \log p_{\mathcal{N}}(\mathbf{z})]$$

To prove Proposition 1, we first introduce the following lemmas:

**Lemma A.1.**

$$\max_{\theta, \phi} \mathcal{L}_{\text{VAE}}(\theta, \phi) \leq \max_{\lambda, \theta, \phi} \mathcal{L}(\lambda, \theta, \phi)$$

*Proof.* Let  $\lambda_0$  be the set of parameters satisfying  $f_{\lambda_0} = \text{id}$  (identity mapping), then  $\frac{\partial f_{\lambda_0}}{\partial \mathbf{z}} = \mathbf{I}$ , and:

$$\begin{aligned} \mathcal{L}(\lambda_0, \theta, \phi) &= \mathbb{E}_{p^*(\mathbf{x})} \mathbb{E}_{q_\phi(\mathbf{z}|\mathbf{x})} \left[ \log p_\theta(\mathbf{x}|\mathbf{z}) - \log q_\phi(\mathbf{z}|\mathbf{x}) + \log \left| \det \left( \frac{\partial f_{\lambda_0}}{\partial \mathbf{z}} \right) \right| + \log p_{\mathcal{N}}(f_{\lambda_0}(\mathbf{z})) \right] \\ &= \mathbb{E}_{p^*(\mathbf{x})} \mathbb{E}_{q_\phi(\mathbf{z}|\mathbf{x})} [\log p_\theta(\mathbf{x}|\mathbf{z}) - \log q_\phi(\mathbf{z}|\mathbf{x}) + \log p_{\mathcal{N}}(\mathbf{z})] \end{aligned}$$

which means  $\mathcal{L}_{\text{VAE}}(\theta, \phi) = \mathcal{L}(\lambda_0, \theta, \phi)$ , thus we have:

$$\mathcal{L}_{\text{VAE}}(\theta, \phi) \leq \max_{\lambda} \mathcal{L}(\lambda, \theta, \phi)$$

Since for all  $\theta$  and  $\phi$ , the above inequality always holds, we have:

$$\max_{\theta, \phi} \mathcal{L}_{\text{VAE}}(\theta, \phi) \leq \max_{\lambda, \theta, \phi} \mathcal{L}(\lambda, \theta, \phi)$$

□

**Lemma A.2.** For all  $\theta, \phi$ ,

$$\mathcal{L}_{\text{VAE}}(\theta, \phi) = \max_{\lambda} \mathcal{L}(\lambda, \theta, \phi)$$

only if  $q_\phi(\mathbf{z}) = p_{\mathcal{N}}(\mathbf{z})$ .

*Proof.* As Lemma A.1 has proved,  $\mathcal{L}_{\text{VAE}}(\theta, \phi) = \mathcal{L}(\lambda_0, \theta, \phi)$ , thus we only need to prove  $\lambda_0$  is not the optimal solution of  $\max_{\lambda} \mathcal{L}(\lambda, \theta, \phi)$ .

We start by introducing a non-parameterized continuous function  $f(\mathbf{z})$ , and rewrite  $\mathcal{L}(\lambda, \theta, \phi)$  as a functional on  $f$ :

$$\mathcal{L}[f] = \mathbb{E}_{p^*(\mathbf{x})} \mathbb{E}_{q_\phi(\mathbf{z}|\mathbf{x})} \left[ \log p_\theta(\mathbf{x}|\mathbf{z}) - \log q_\phi(\mathbf{z}|\mathbf{x}) + \log \left| \det \left( \frac{\partial f}{\partial \mathbf{z}} \right) \right| + \log p_{\mathcal{N}}(f(\mathbf{z})) \right]$$

According to Hornik [12], neural networks can represent any continuous function defined on  $\mathbb{R}^n$ . If we can find a continuous differentiable function  $f(\mathbf{z})$ , which will give  $\mathcal{L}[f] > \mathcal{L}_{\text{VAE}}(\theta, \phi)$ , then there must exist a neural network derived  $f_\lambda(\mathbf{z}) = f(\mathbf{z})$ , s.t.  $\mathcal{L}(\lambda, \theta, \phi) > \mathcal{L}(\lambda_0, \theta, \phi)$ . Because of this, although we can only apply calculus of variations on continuous differentiable functions, it is sufficient to prove Lemma A.2 with this method. We write  $\mathcal{L}[f]$  into the form of Euler's equation:

$$\mathcal{L}[f] = \int F\left(\mathbf{z}, f, \frac{\partial f}{\partial \mathbf{z}}\right) d\mathbf{z}$$

where

$$\begin{aligned} &F\left(\mathbf{z}, f, \frac{\partial f}{\partial \mathbf{z}}\right) \\ &= \int p^*(\mathbf{x}) q_\phi(\mathbf{z}|\mathbf{x}) \left[ \log p_\theta(\mathbf{x}|\mathbf{z}) - \log q_\phi(\mathbf{z}|\mathbf{x}) + \log \left| \det \left( \frac{\partial f}{\partial \mathbf{z}} \right) \right| + \log p_{\mathcal{N}}(f(\mathbf{z})) \right] d\mathbf{x} \\ &= \int p^*(\mathbf{x}) q_\phi(\mathbf{z}|\mathbf{x}) \left[ \log p_\theta(\mathbf{x}|\mathbf{z}) - \log q_\phi(\mathbf{z}|\mathbf{x}) + \log \left| \det \left( \frac{\partial f}{\partial \mathbf{z}} \right) \right| + \sum_k \log p_{\mathcal{N}}(f^i(\mathbf{z})) \right] d\mathbf{x} \end{aligned}$$

Here we use  $f^i(\mathbf{z})$  to denote the  $i$ -th dimension of the output of  $f(\mathbf{z})$ , while  $x_j$  and  $z_j$  to denote the  $j$ -th dimension of  $\mathbf{x}$  and  $\mathbf{z}$ . For  $\log |\det(\partial f / \partial \mathbf{z})|$ , we can further expand it *w.r.t.* the  $k$ -th row:

$$\log \left| \det \left( \frac{\partial f}{\partial \mathbf{z}} \right) \right| = \log \left[ \sum_j \frac{\partial f^i}{\partial z_j} (-1)^{i+j} M_{ij} \right]$$

where  $M_{ij}$  is the  $(i, j)$  minor of the Jacobian matrix  $\partial f / \partial \mathbf{z}$ .

Assume we have  $\mathcal{L}_{\text{VAE}}(\theta, \phi) = \max_{\lambda} \mathcal{L}(\lambda, \theta, \phi)$ . That is,  $\mathcal{L}[f]$  attains its extremum at  $f = f_{\lambda_0} = \text{id}$ , or:

$$\frac{\delta L}{\delta f} = 0 \quad (\text{A.1})$$

According to Euler's equation [8, page 14 and 35], the necessary condition for Eq. (A.1) is:

$$\frac{\partial F}{\partial f^i} - \sum_j \frac{\partial}{\partial z_j} \frac{\partial F}{\partial (\partial_{z_j} f^i)} = 0 \quad (\text{A.2})$$

for all  $i$ . Note we use  $\partial_{z_j} f^i$  to denote  $\frac{\partial f^i}{\partial z_j}$ .

Consider the term  $\frac{\partial F}{\partial f^i}$ , we have:

$$\frac{\partial F}{\partial f^i} = \int p^*(\mathbf{x}) q_{\phi}(\mathbf{z}|\mathbf{x}) \cdot \frac{1}{p_{\mathcal{N}}(f^i(\mathbf{z}))} \cdot \frac{\partial p_{\mathcal{N}}(f^i(\mathbf{z}))}{\partial f^i} d\mathbf{x}$$

where  $p_{\mathcal{N}}(f^i(\mathbf{z})) = \frac{1}{\sqrt{2\pi}} \exp \left[ -\frac{(f^i(\mathbf{z}))^2}{2} \right]$ , thus we have:

$$\frac{\partial p_{\mathcal{N}}(f^i(\mathbf{z}))}{\partial f^i} = \frac{1}{\sqrt{2\pi}} \exp \left[ -\frac{(f^i(\mathbf{z}))^2}{2} \right] \cdot (-f^i(\mathbf{z})) = -p_{\mathcal{N}}(f^i(\mathbf{z})) f^i(\mathbf{z})$$

Therefore,

$$\frac{\partial F}{\partial f^i} = \int p^*(\mathbf{x}) q_{\phi}(\mathbf{z}|\mathbf{x}) \cdot \frac{1}{p_{\mathcal{N}}(f^i(\mathbf{z}))} \cdot [-p_{\mathcal{N}}(f^i(\mathbf{z})) f^i(\mathbf{z})] d\mathbf{x} = \int -p^*(\mathbf{x}) q_{\phi}(\mathbf{z}|\mathbf{x}) f^i(\mathbf{z}) d\mathbf{x} \quad (\text{A.3})$$

Consider the other term  $\sum_j \frac{\partial}{\partial z_j} \frac{\partial F}{\partial (\partial_{z_j} f^i)}$ ,

$$\begin{aligned} \frac{\partial F}{\partial (\partial_{z_j} f^i)} &= \int \frac{\partial (p^*(\mathbf{x}) q_{\phi}(\mathbf{z}|\mathbf{x}) \log |\det(\partial f / \partial \mathbf{z})|)}{\partial (\partial_{z_j} f^i)} d\mathbf{x} \\ &= \int p^*(\mathbf{x}) q_{\phi}(\mathbf{z}|\mathbf{x}) \frac{\partial \left( \log \left[ \sum_k \frac{\partial f^i}{\partial z_k} (-1)^{i+k} M_{ik} \right] \right)}{\partial (\partial_{z_j} f^i)} d\mathbf{x} \\ &= \int p^*(\mathbf{x}) q_{\phi}(\mathbf{z}|\mathbf{x}) \cdot \frac{1}{|\det(\partial f / \partial \mathbf{z})|} \cdot (-1)^{i+j} M_{ij} d\mathbf{x} \end{aligned}$$

Since  $f = \text{id}$ , we have  $\partial f / \partial \mathbf{z} = \mathbf{I}$ , thus  $\partial f / \partial \mathbf{z}$  is independent on  $z_j$ , and:

$$\frac{\partial}{\partial z_j} \frac{\partial F}{\partial (\partial_{z_j} f^i)} = \int \frac{\partial q_{\phi}(\mathbf{z}|\mathbf{x})}{\partial z_j} \cdot p^*(\mathbf{x}) \cdot \frac{1}{|\det(\partial f / \partial \mathbf{z})|} \cdot (-1)^{i+j} M_{ij} d\mathbf{x} \quad (\text{A.4})$$

$$M_{ij} = \delta_{ij} = \begin{cases} 1, & \text{if } i = j \\ 0, & \text{otherwise} \end{cases} \quad (\text{A.5})$$

Substitute Eq. (A.3), (A.4) and (A.5) into Eq. (A.2), we have:

$$\int -p^*(\mathbf{x}) q_{\phi}(\mathbf{z}|\mathbf{x}) f^i(\mathbf{z}) d\mathbf{x} - \sum_j \left[ \frac{\partial q_{\phi}(\mathbf{z}|\mathbf{x})}{\partial z_j} \cdot p^*(\mathbf{x}) \cdot (-1)^{i+j} \delta_{ij} \right] d\mathbf{x} = 0$$

We then have:

$$\begin{aligned}
& \int -p^*(\mathbf{x}) q_\phi(\mathbf{z}|\mathbf{x}) z_i - \frac{\partial q_\phi(\mathbf{z}|\mathbf{x})}{\partial z_i} \cdot p^*(\mathbf{x}) \cdot (-1)^{i+1} \delta_{ii} d\mathbf{x} = 0 \\
\Rightarrow & \int -p^*(\mathbf{x}) q_\phi(\mathbf{z}|\mathbf{x}) z_i - \frac{\partial q_\phi(\mathbf{z}|\mathbf{x})}{\partial z_i} p^*(\mathbf{x}) d\mathbf{x} = 0 \\
\Rightarrow & z_i \int -p^*(\mathbf{x}) q_\phi(\mathbf{z}|\mathbf{x}) d\mathbf{x} = \int \frac{\partial q_\phi(\mathbf{z}|\mathbf{x})}{\partial z_i} p^*(\mathbf{x}) d\mathbf{x} \\
\Rightarrow & z_i \int -p^*(\mathbf{x}) q_\phi(\mathbf{z}|\mathbf{x}) d\mathbf{x} = \frac{\partial}{\partial z_i} \int q_\phi(\mathbf{z}|\mathbf{x}) p^*(\mathbf{x}) d\mathbf{x} \\
\Rightarrow & -z_i \cdot q_\phi(\mathbf{z}) = \frac{\partial}{\partial z_i} q_\phi(\mathbf{z})
\end{aligned}$$

Let  $q_\phi(\mathbf{z}) = q_\phi(z_1|z_2, \dots, z_K) \cdot q_\phi(z_2, \dots, z_K)$ , where  $K$  is the number of dimensions of  $\mathbf{z}$ . We shall first solve the differential equation w.r.t.  $z_1$ :

$$\begin{aligned}
& -z_1 \cdot q_\phi(\mathbf{z}) = \frac{\partial}{\partial z_1} q_\phi(\mathbf{z}) \tag{A.6} \\
\Rightarrow & -z_1 \cdot q_\phi(z_1|z_2, \dots, z_K) \cdot q_\phi(z_2, \dots, z_K) = \frac{\partial}{\partial z_1} q_\phi(z_1|z_2, \dots, z_K) \cdot q_\phi(z_2, \dots, z_K) \\
\Rightarrow & -z_1 \cdot q_\phi(z_1|z_2, \dots, z_K) \cdot q_\phi(z_2, \dots, z_K) = q_\phi(z_2, \dots, z_K) \cdot \frac{\partial}{\partial z_1} q_\phi(z_1|z_2, \dots, z_K) \\
\Rightarrow & -z_1 \cdot q_\phi(z_1|z_2, \dots, z_K) = \frac{\partial}{\partial z_1} q_\phi(z_1|z_2, \dots, z_K) \\
\Rightarrow & -z_1 \frac{\partial}{\partial z_1} q_\phi(z_1|z_2, \dots, z_K) = \frac{\partial}{\partial z_1} q_\phi(z_1|z_2, \dots, z_K) \\
\Rightarrow & \int -z_1 \frac{\partial}{\partial z_1} q_\phi(z_1|z_2, \dots, z_K) = \int \frac{\partial}{\partial z_1} q_\phi(z_1|z_2, \dots, z_K) \\
\Rightarrow & -\frac{1}{2} z_1^2 + C(z_2, \dots, z_K) = \log q_\phi(z_1|z_2, \dots, z_K) \\
\Rightarrow & \exp\left(-\frac{1}{2} z_1^2\right) \cdot \exp(C(z_2, \dots, z_K)) = q_\phi(z_1|z_2, \dots, z_K)
\end{aligned}$$

Since  $q_\phi(z_1|z_2, \dots, z_K)$  is a probability distribution, we have:

$$\exp(C(z_2, \dots, z_K)) = \frac{1}{\int \exp\left(-\frac{1}{2} z_1^2\right) dz_1} = \frac{1}{\sqrt{2\pi}}$$

thus we have:

$$q_\phi(\mathbf{z}) = q_\phi(z_1|z_2, \dots, z_K) \cdot q_\phi(z_2, \dots, z_K) = \frac{1}{\sqrt{2\pi}} \exp\left(-\frac{1}{2} z_1^2\right) \cdot q_\phi(z_2, \dots, z_K)$$

We then solve the differential equation w.r.t.  $z_2$ :

$$\begin{aligned}
& -z_2 \cdot q_\phi(\mathbf{z}) = \frac{\partial}{\partial z_2} q_\phi(\mathbf{z}) \\
\Rightarrow & -z_2 \cdot \frac{1}{\sqrt{2\pi}} \exp\left(-\frac{1}{2} z_1^2\right) \cdot q_\phi(z_2, \dots, z_K) = \frac{\partial}{\partial z_2} \frac{1}{\sqrt{2\pi}} \exp\left(-\frac{1}{2} z_1^2\right) \cdot q_\phi(z_2, \dots, z_K) \\
\Rightarrow & -z_2 \cdot \frac{1}{\sqrt{2\pi}} \exp\left(-\frac{1}{2} z_1^2\right) \cdot q_\phi(z_2, \dots, z_K) = \frac{1}{\sqrt{2\pi}} \exp\left(-\frac{1}{2} z_1^2\right) \cdot \frac{\partial}{\partial z_2} q_\phi(z_2, \dots, z_K) \\
\Rightarrow & -z_2 \cdot q_\phi(z_2, \dots, z_K) = \frac{\partial}{\partial z_2} q_\phi(z_2, \dots, z_K) \tag{A.7}
\end{aligned}$$

If we let  $\mathbf{z}' = z_2, \dots, z_K$ , the form of Eq. (A.7) is now exactly identical with Eq. (A.6). Use the same method, we can solve the equation w.r.t.  $z_2$ , and further w.r.t.  $z_3, \dots, z_K$ . Finally, we can get the solution:

$$q_\phi(\mathbf{z}) = \frac{1}{(\sqrt{2\pi})^K} \prod_{i=1}^K \exp\left(-\frac{1}{2} z_i^2\right)$$

which is  $K$ -dimensional unit Gaussian, i.e.,  $q_\phi(\mathbf{z}) = p_{\mathcal{N}}(\mathbf{z})$ .  $\square$

**Lemma A.3.** For all  $\theta, \phi$ , if  $q_\phi(\mathbf{z}) \neq p_{\mathcal{N}}(\mathbf{z})$ ,  $\exists f_\lambda \neq f_{\lambda_0}$ , s.t.  $\mathcal{L}(\lambda, \theta, \phi) > \mathcal{L}(\lambda_0, \theta, \phi)$ .

*Proof.* If  $q_\phi(\mathbf{z}) \neq p_\lambda(\mathbf{z})$ , then according to Eq. (A.1), we have:

$$\left. \frac{\delta \mathcal{L}}{\delta f} \right|_{f=f_{\lambda_0}} \neq 0$$

Then there must exist  $f_\lambda$  in the neighborhood of  $f_{\lambda_0}$ , such that  $\mathcal{L}(\lambda, \theta, \phi) > \mathcal{L}(\lambda_0, \theta, \phi)$ .  $\square$

Finally, we get to the proof for Proposition 1:

**Proposition.** For VAE with flow prior  $p_\lambda(\mathbf{z}) = p_{\mathcal{N}}(f_\lambda(\mathbf{z})) |\det(\partial f_\lambda / \partial \mathbf{z})|$ , where  $p_{\mathcal{N}}(f_\lambda(\mathbf{z})) = \mathcal{N}(\mathbf{0}, \mathbf{I})$ , if  $q_\phi(\mathbf{z}) \neq \mathcal{N}(\mathbf{0}, \mathbf{I})$ , then its training objective (elbo):

$$\mathcal{L}(\lambda, \theta, \phi) = \mathbb{E}_{p^*(\mathbf{x})} \mathbb{E}_{q_\phi(\mathbf{z}|\mathbf{x})} \left[ \log p_\theta(\mathbf{x}|\mathbf{z}) + \log p_{\mathcal{N}}(f_\lambda(\mathbf{z})) + \log \left| \det \left( \frac{\partial f_\lambda(\mathbf{z})}{\partial \mathbf{z}} \right) \right| - \log q_\phi(\mathbf{z}|\mathbf{x}) \right]$$

can reach its extremum only if  $f_\lambda \neq f_{\lambda_0}$ , where  $f_{\lambda_0} = \text{id}$  is the identity mapping. Also,  $\forall \theta, \phi$ , if  $q_\phi(\mathbf{z}) \neq \mathcal{N}(\mathbf{0}, \mathbf{I})$ , then there exist  $f_\lambda \neq f_{\lambda_0}$ , s.t.  $\mathcal{L}(\lambda, \theta, \phi) > \mathcal{L}(\lambda_0, \theta, \phi)$ .

*Proof. Necessity* According to Lemma A.2,  $\mathcal{L}_{\text{VAE}}(\theta, \phi) = \max_\lambda \mathcal{L}(\lambda, \theta, \phi)$  implies  $q_\phi(\mathbf{z}) = p_{\mathcal{N}}(\mathbf{z})$ . Take Lemma A.1 into consideration, it means if  $q_\phi(\mathbf{z}) \neq p_{\mathcal{N}}(\mathbf{z})$ , then  $\forall \theta, \phi$ ,  $\mathcal{L}_{\text{VAE}}(\theta, \phi) = \mathcal{L}(\lambda_0, \theta, \phi) < \max_\lambda \mathcal{L}(\lambda, \theta, \phi)$ . Hence,  $f_\lambda \neq f_{\lambda_0}$  is the necessary condition for  $\mathcal{L}(\lambda, \theta, \phi)$  to reach its extremum if  $q_\phi(\mathbf{z}) \neq p_{\mathcal{N}}(\mathbf{z})$ .

**Effectiveness** According to Lemma A.3, there always exist a  $f_\lambda \neq f_{\lambda_0}$  when  $q_\phi(\mathbf{z}) \neq p_\lambda(\mathbf{z})$ , s.t.  $\mathcal{L}(\lambda, \theta, \phi) > \mathcal{L}(\lambda_0, \theta, \phi) = \mathcal{L}_{\text{VAE}}(\theta, \phi)$ .  $\square$

## A.2 Proof for Proposition 2

*Proof.* To apply calculus of variations, we need to substitute the parameterized, bounded  $\mu_\theta(\mathbf{z})$  with a non-parameterized, unbounded mapping. Since  $0 < \mu_\theta^k(\mathbf{z}) < 1$ , and  $\mu_\theta(\mathbf{z})$  is produced by neural network, which ensures  $\mu_\theta(\mathbf{z})$  is a continuous mapping, then  $\forall \theta$ , there exists unbounded  $\mathbf{t}(\mathbf{z})$ , s.t.

$$\begin{aligned} \mu_\theta^k(\mathbf{z}) &= \frac{\exp(t^k(\mathbf{z}))}{1 + \exp(t^k(\mathbf{z}))} \\ t^k(\mathbf{z}) &= \log \mu_\theta^k(\mathbf{z}) - \log(1 - \mu_\theta^k(\mathbf{z})) \end{aligned}$$

and for all continuous mapping  $\mathbf{t}(\mathbf{z})$ , there also exists  $\mu_\theta(\mathbf{z})$ , satisfying the above equations. In fact, this substitution is also adopted in the actual implementation of our models.

The probability of  $p_\theta(\mathbf{x}|\mathbf{z})$  is given by:

$$p_\theta(\mathbf{x}|\mathbf{z}) = \text{Bernoulli}(\mu_\theta(\mathbf{z})) = \prod_k (\mu_\theta^k(\mathbf{z}))^{x_k} (1 - \mu_\theta^k(\mathbf{z}))^{(1-x_k)}$$

Then we have:

$$\begin{aligned} \log p_\theta(\mathbf{x}|\mathbf{z}) &= \sum_k \left\{ x_k \log \mu_\theta^k(\mathbf{z}) + (1 - x_k) \log (1 - \mu_\theta^k(\mathbf{z})) \right\} \\ &= \sum_k \left\{ x_k t^k(\mathbf{z}) - x_k \log [1 + \exp(t^k(\mathbf{z}))] - (1 - x_k) \log [1 + \exp(t^k(\mathbf{z}))] \right\} \\ &= \sum_k \left\{ x_k t^k(\mathbf{z}) - \log [1 + \exp(t^k(\mathbf{z}))] \right\} \end{aligned}$$

The training objective  $\mathcal{L}$  can be then formulated as a functional on  $\mathbf{t}(\mathbf{z})$ :

$$\begin{aligned} \mathcal{L}[\mathbf{t}] &= \mathbb{E}_{p^*(\mathbf{x})} \mathbb{E}_{q_\phi(\mathbf{z}|\mathbf{x})} \left[ \log p_\theta(\mathbf{x}|\mathbf{z}) + \log \frac{p_\theta(\mathbf{z})}{q_\phi(\mathbf{z}|\mathbf{x})} \right] \\ &= \iint p^*(\mathbf{x}) q_\phi(\mathbf{z}|\mathbf{x}) \left( \log p_\theta(\mathbf{x}|\mathbf{z}) + \log \frac{p_\theta(\mathbf{z})}{q_\phi(\mathbf{z}|\mathbf{x})} \right) d\mathbf{z} d\mathbf{x} \\ &= \int F(\mathbf{z}, \mathbf{t}) d\mathbf{z} \end{aligned}$$

where  $F(\mathbf{z}, \mathbf{t})$  is:

$$F(\mathbf{z}, \mathbf{t}) = \int p^*(\mathbf{x}) q_\phi(\mathbf{z}|\mathbf{x}) \left[ \sum_k \left\{ x_k t^k(\mathbf{z}) - \log [1 + \exp(t^k(\mathbf{z}))] \right\} + \log \frac{p_\theta(\mathbf{z})}{q_\phi(\mathbf{z}|\mathbf{x})} \right] d\mathbf{x}$$

According to Euler's equation [8, page 14 and 35], the necessary condition for  $\mathcal{L}[\mathbf{t}]$  to have an extremum for a given  $\mathbf{t}(\mathbf{z})$  is that,  $\mathbf{t}(\mathbf{z})$  satisfies  $\partial F / \partial t^k = 0, \forall k$ . Thus we have:

$$\begin{aligned} \frac{\partial F}{\partial t^k} = 0 &\implies \int p^*(\mathbf{x}) q_\phi(\mathbf{z}|\mathbf{x}) \left[ x_k - \frac{\exp(t^k(\mathbf{z}))}{1 + \exp(t^k(\mathbf{z}))} \right] d\mathbf{x} = 0 \\ &\implies \int p^*(\mathbf{x}) q_\phi(\mathbf{z}|\mathbf{x}) [x_k - \mu_\theta^k(\mathbf{z})] d\mathbf{x} = 0 \\ &\implies \sum_i q_\phi(\mathbf{z}|\mathbf{x}^{(i)}) [x_k^{(i)} - \mu_\theta^k(\mathbf{z})] = 0 \\ &\implies \sum_i q_\phi(\mathbf{z}|\mathbf{x}^{(i)}) x_k^{(i)} = \left( \sum_i q_\phi(\mathbf{z}|\mathbf{x}^{(i)}) \right) \mu_\theta^k(\mathbf{z}) \\ &\implies \mu_\theta^k(\mathbf{z}) = \frac{\sum_i q_\phi(\mathbf{z}|\mathbf{x}^{(i)}) x_k^{(i)}}{\sum_j q_\phi(\mathbf{z}|\mathbf{x}^{(j)})} \end{aligned}$$

That is to say,  $\mu_\theta(\mathbf{z}) = \frac{\sum_i q_\phi(\mathbf{z}|\mathbf{x}^{(i)}) \mathbf{x}^{(i)}}{\sum_j q_\phi(\mathbf{z}|\mathbf{x}^{(j)})} = \sum_i w_i(\mathbf{z}) \mathbf{x}^{(i)}$ .  $\square$

Rezende and Viola [26] has proved that when  $p_\theta(\mathbf{x}|\mathbf{z}) = \mathcal{N}(\mu_\theta(\mathbf{z}), \sigma^2 \mathbf{I})$ , where  $\sigma$  is a global fixed constant, the optimal decoder  $\mu_\theta(\mathbf{z}) = \sum_i w_i(\mathbf{z}) \mathbf{x}^{(i)}$ , which is exactly the same as our conclusion. Rosca et al. [28] has proved that the gradient of Bernoulli( $\mu_\theta(\mathbf{z})$ ) is the same as  $\mathcal{N}(\mu_\theta(\mathbf{z}), \sigma^2 \mathbf{I})$  when  $\sigma = 1$ , but they did not calculate out the optimal decoder. We push forward both these works.

### A.3 Trade-off between reconstruction loss and mutual information

To show there is a trade-off between *reconstruction loss* and *mutual information*, we first assume the *mutual information*  $\mathbb{I}_\phi[Z; X]$  reaches its optimum value. Since

$$\mathbb{I}_\phi[Z; X] = \iint q_\phi(\mathbf{z}, \mathbf{x}) \log \frac{q_\phi(\mathbf{z}, \mathbf{x})}{q_\phi(\mathbf{z}) p^*(\mathbf{x})} d\mathbf{z} d\mathbf{x} = D_{KL}[q_\phi(\mathbf{z}, \mathbf{x}) \| q_\phi(\mathbf{z}) p^*(\mathbf{x})]$$

we can see that  $\mathbb{I}_\phi[Z; X]$  reaches its minimum value 0 if and only if  $q_\phi(\mathbf{z}, \mathbf{x}) = q_\phi(\mathbf{z}) p^*(\mathbf{x})$ . This means  $q_\phi(\mathbf{z}|\mathbf{x}) = q_\phi(\mathbf{z})$  for all  $\mathbf{x}$  and  $\mathbf{z}$ , since  $q_\phi(\mathbf{z}, \mathbf{x}) = q_\phi(\mathbf{z}|\mathbf{x}) p^*(\mathbf{x})$ . According to Proposition 2, we then have:

$$\mu_\theta(\mathbf{z}) = \frac{\sum_i q_\phi(\mathbf{z}|\mathbf{x}^{(i)}) \mathbf{x}^{(i)}}{\sum_j q_\phi(\mathbf{z}|\mathbf{x}^{(j)})} = \frac{\sum_i q_\phi(\mathbf{z}) \mathbf{x}^{(i)}}{\sum_j q_\phi(\mathbf{z})} = \frac{1}{N} \sum_i \mathbf{x}^{(i)}$$

this means the decoder  $\mu_\theta(\mathbf{z})$  will produce the same reconstruction output for all  $\mathbf{z}$ , which is the average of all training data, hence causing a poor *reconstruction loss*.

The fact that *mutual information* can reach its optimum value only when having a poor *reconstruction loss* indicates there is trade-off between *reconstruction loss* and *mutual information*.

## B Experimental details

### B.1 Datasets

**MNIST** MNIST is a 28x28 grayscale image dataset of hand-written digits, with 60,000 data points for training and 10,000 for testing. When validation is required for early-stopping, we randomly split the training data into 50,000 for training and 10,000 for validation.

Since we use Bernoulli  $p_\theta(\mathbf{x}|\mathbf{z})$  to model these images in VAE, we binarize these images by the method in [29]: each pixel value is randomly set to 1 in proportion to its pixel intensity. The

training and validation images are re-binarized at each epoch. However, the test images are binarized beforehand for all experiments. We binarize each test image 10 times, and use all these 10 binarized data points in evaluation. This method results in a 10 times larger test set, but we believe this can help us to obtain a more objective evaluation result.

**StaticMNIST** StaticMNIST [19] is a pre-binarized MNIST image dataset, with the original 60,000 training data already splitted into 50,000 for training and 10,000 for validation. We always use validation set for early-stopping on StaticMNIST. Meanwhile, since StaticMNIST has already been binarized, the test set is used as-is without 10x enlargement.

**FashionMNIST** FashionMNIST [37] is a recently proposed image dataset of grayscale fashion products, with the same specification as MNIST. We thus use the same training-validation split and the same binarization method just as MNIST.

**Omniglot** Omniglot [18] is a 28x28 grayscale image dataset of hand-written characters. We use the preprocessed data from [4], with 24,345 data points for training and 8,070 for testing. When validation is required, we randomly split the training data into 20,345 for training and 4,000 for validation. We use dynamic binarization on Omniglot just as MNIST.

## B.2 Network architectures

**Notations** In order to describe the detailed architecture of our models, we will introduce auxiliary functions to denote network components. A function  $h_\phi(\mathbf{x})$  should denote a sub-network in  $q_\phi(\mathbf{z}|\mathbf{x})$ , with a subset of  $\phi$  as its own learnable parameters. For example, if we write  $q_\phi(\mathbf{z}|\mathbf{x}) = q_\phi(\mathbf{z}|h_\phi(\mathbf{x})) = \mathcal{N}(\boldsymbol{\mu}_\phi(h_\phi(\mathbf{x})), \boldsymbol{\sigma}_\phi^2(h_\phi(\mathbf{x})) \mathbf{I})$ , it means that the posterior  $q_\phi(\mathbf{z}|\mathbf{x})$  is a Gaussian, whose mean and standard deviation are derived by one shared sub-network  $h_\phi(\mathbf{x})$  and two separated sub-networks  $\boldsymbol{\mu}_\phi(\cdot)$  and  $\boldsymbol{\sigma}_\phi(\cdot)$ , respectively.

The structure of a network is described by composition of elementary neural network layers.

Linear[ $k$ ] indicates a linear dense layer with  $k$  outputs. Dense[ $k$ ] indicates a non-linear dense layer.  $a \rightarrow b$  indicates a composition of  $a$  and  $b$ , e.g.,  $\text{Dense}[m] \rightarrow \text{Dense}[n]$  indicates two successive dense layers, while the first layer has  $m$  outputs and the second layer has  $n$  outputs. These two dense layers can also be abbreviated as Dense[ $m \rightarrow n$ ].

Conv[ $H \times W \times C$ ] denotes a non-linear convolution layer, whose output shape is  $H \times W \times C$ , where  $H$  is the height,  $W$  is the width and  $C$  is the channel size. As abbreviation, Conv[ $H_1 \times W_1 \times C_1 \rightarrow H_2 \times W_2 \times C_2$ ] denotes two successive non-linear convolution layers. Resnet[.] denotes non-linear resnet layer(s) [38]. All Conv and Resnet layers by default use 3x3 kernels, unless the kernel size is specified as subscript (e.g., Conv<sub>1x1</sub> denotes a 1x1 convolution layer). The strides of Conv and Resnet layers are automatically determined by the input and output shapes, which is 2 in most cases. LinearConv[.] denotes linear convolution layer(s).

DeConv[.] and DeResnet[.] denotes deconvolution and deconvolutional resnet layers, respectively.

PixelCNN[.] is a PixelCNN layer proposed by Salimans et al. [31]. It uses resnet layers, instead of convolution layers. Details can be found in its original paper.

Flatten indicates to reshape the input 3-d tensor into a vector, while UnFlatten[ $H \times W \times C$ ] indicates to reshape the input vector into a 3-d tensor of shape  $H \times W \times C$ . Concat[ $a, b$ ] indicates to concat the output of  $a$  and  $b$  along the last axis.

CouplingLayer and ActNorm are components of Real NVP, proposed by Dinh et al. [7] and Kingma and Dhariwal [17]. InvertibleDense is a component modified from *invertible 1x1 convolution* [17]. We shall only introduce the details of CouplingLayer, since it contains sub-networks, while the rest two are just simple components.

**General configurations** All non-linear layers use *leaky relu* [21] activation.

The observed variable  $\mathbf{x}$  (i.e., the input image) is always a 3-d tensor, with shape  $H \times W \times C$ , whether or not the model is convolutional. The latent variable  $\mathbf{z}$  is a vector, whose number of dimensions is chosen to be 40 on MNIST and StaticMNIST, while 64 on FashionMNIST and Omniglot. This is



because we think the latter two datasets are conceptually more complicated than the other two, thus requiring higher dimensional latent variables.

The Gaussian posterior  $q_\phi(\mathbf{z}|\mathbf{x})$  is derived as:

$$\begin{aligned} q_\phi(\mathbf{z}|\mathbf{x}) &= \mathcal{N}(\boldsymbol{\mu}_\phi(h_\phi(\mathbf{x})), \boldsymbol{\sigma}_\phi^2(h_\phi(\mathbf{x})) \mathbf{I}) \\ \boldsymbol{\mu}_\phi(h_\phi(\mathbf{x})) &= h_\phi(\mathbf{x}) \rightarrow \text{Linear}[\text{Dim}(\mathbf{z})] \\ \log \boldsymbol{\sigma}_\phi(h_\phi(\mathbf{x})) &= h_\phi(\mathbf{x}) \rightarrow \text{Linear}[\text{Dim}(\mathbf{z})] \end{aligned}$$

Note we make the network to produce  $\log \boldsymbol{\sigma}_\phi(h_\phi(\mathbf{x}))$  instead of directly producing  $\boldsymbol{\sigma}_\phi(h_\phi(\mathbf{x}))$ .  $h_\phi(\mathbf{x})$  is the hidden layers, varying among different models.

For binarized images, we use Bernoulli conditional distribution  $p_\theta(\mathbf{x}|\mathbf{z})$ , derived as:

$$\begin{aligned} p_\theta(\mathbf{x}|\mathbf{z}) &= \text{Bernoulli}[\boldsymbol{\mu}_\theta(h_\theta(\mathbf{z}))] \\ \log \frac{\boldsymbol{\mu}_\theta(h_\theta(\mathbf{z}))}{1 - \boldsymbol{\mu}_\theta(h_\theta(\mathbf{z}))} &= \begin{cases} h_\theta(\mathbf{z}) \rightarrow \text{Linear}[784] \rightarrow \text{UnFlatten}[28 \times 28 \times 1] & \text{for DenseVAE} \\ h_\theta(\mathbf{z}) \rightarrow \text{LinearConv}_{1 \times 1}[28 \times 28 \times 1] & \text{otherwise} \end{cases} \end{aligned}$$

Note we make the network to produce  $\log \frac{\boldsymbol{\mu}_\theta(h_\theta(\mathbf{z}))}{1 - \boldsymbol{\mu}_\theta(h_\theta(\mathbf{z}))}$ , the *logits* of Bernoulli distribution, instead of producing the Bernoulli mean  $\boldsymbol{\mu}_\theta(h_\theta(\mathbf{z}))$  directly.

**DenseVAE**  $h_\phi(\mathbf{x})$  and  $h_\theta(\mathbf{z})$  of DenseVAE are composed of dense layers, formulated as:

$$\begin{aligned} h_\phi(\mathbf{x}) &= \mathbf{x} \rightarrow \text{Flatten} \rightarrow \text{Dense}[500 \rightarrow 500] \\ h_\theta(\mathbf{z}) &= \mathbf{z} \rightarrow \text{Dense}[500 \rightarrow 500] \end{aligned}$$

**Conv/ResnetVAE**  $h_\phi(\mathbf{x})$  and  $h_\theta(\mathbf{z})$  of ConvVAE are composed of (de)convolutional layers, while those of ResnetVAE consist of (deconvolutional) resnet layers. We only describe the architecture of ResnetVAE here. The structure of ConvVAE can be easily obtained by replacing all (deconvolutional) resnet layers with (de)convolution layers:

$$\begin{aligned} h_\phi(\mathbf{x}) &= \mathbf{x} \rightarrow \text{Resnet}[28 \times 28 \times 32 \rightarrow 28 \times 28 \times 32 \rightarrow 14 \times 14 \times 64 \\ &\quad \rightarrow 14 \times 14 \times 64 \rightarrow 7 \times 7 \times 64 \rightarrow 7 \times 7 \times 16] \\ &\quad \rightarrow \text{Flatten} \\ h_\theta(\mathbf{z}) &= \mathbf{z} \rightarrow \text{Dense}[784] \rightarrow \text{UnFlatten}[7 \times 7 \times 16] \\ &\quad \rightarrow \text{DeResnet}[7 \times 7 \times 64 \rightarrow 14 \times 14 \times 64 \rightarrow 14 \times 14 \times 64 \\ &\quad \rightarrow 28 \times 28 \times 32 \rightarrow 28 \times 28 \times 32] \end{aligned}$$

**PixelVAE**  $h_\phi(\mathbf{x})$  of PixelVAE is the exactly same as ResnetVAE, while  $h_\theta(\mathbf{z})$  is derived as:

$$\begin{aligned} h_\theta(\mathbf{z}) &= \text{Concat}[\mathbf{x}, \tilde{h}_\theta(\mathbf{z})] \\ &\quad \rightarrow \text{PixelCNN}[28 \times 28 \times 33 \rightarrow 28 \times 28 \times 33 \rightarrow 28 \times 28 \times 33] \\ \tilde{h}_\theta(\mathbf{z}) &= \mathbf{z} \rightarrow \text{Dense}[784] \rightarrow \text{UnFlatten}[7 \times 7 \times 16] \\ &\quad \rightarrow \text{DeResnet}[7 \times 7 \times 64 \rightarrow 14 \times 14 \times 64 \rightarrow 14 \times 14 \times 64 \\ &\quad \rightarrow 28 \times 28 \times 32 \rightarrow 28 \times 28 \times 32] \end{aligned}$$

As Salimans et al. [31], we use dropout in PixelCNN layers, with rate 0.5.

**Real NVP** The RNVP consists of  $K$  blocks, while each block consist of an *invertible dense*, a *coupling layer*, and an *actnorm*. The Real NVP mapping for prior, i.e.  $f_\lambda(\mathbf{z})$ , can be formulated as:

$$\begin{aligned} f_\lambda(\mathbf{z}) &= \mathbf{z} \rightarrow f_1(\mathbf{h}_1) \rightarrow \cdots \rightarrow f_K(\mathbf{h}_K) \\ f_k(\mathbf{h}_k) &= \mathbf{h}_k \rightarrow \text{InvertibleDense} \rightarrow \text{CouplingLayer} \rightarrow \text{ActNorm} \\ \text{CouplingLayer}(\mathbf{u}) &= \text{Concat}[\mathbf{u}_l, \mathbf{u}_r \odot \text{Sigmoid}(s_\lambda(h_{\lambda,k}(\mathbf{u}_l))) + t_\lambda(h_{\lambda,k}(\mathbf{u}_l))] \\ h_{\lambda,k}(\mathbf{u}_l) &= \mathbf{u}_l \rightarrow \text{Dense}[256] \\ s_\lambda(h_{\lambda,k}(\mathbf{u}_l)) &= h_{\lambda,k}(\mathbf{u}_l) \rightarrow \text{Linear}[\text{Dim}(\mathbf{u}_r)] \\ t_\lambda(h_{\lambda,k}(\mathbf{u}_l)) &= h_{\lambda,k}(\mathbf{u}_l) \rightarrow \text{Linear}[\text{Dim}(\mathbf{u}_r)] \end{aligned}$$

where  $\mathbf{u}_l = \mathbf{u}_{0:\lfloor \text{Dim}(\mathbf{u})/2 \rfloor}$  is the left half of  $\mathbf{u}$ , and  $\mathbf{u}_r = \mathbf{u}_{\lfloor \text{Dim}(\mathbf{u})/2 \rfloor:\text{Dim}(\mathbf{u})}$  is the right half.

The RNVP posterior, derived from the original Gaussian posterior  $q_\phi(\mathbf{w}|\mathbf{x})$ , is denoted as  $q_{\phi,\eta}(\mathbf{z}|\mathbf{x})$ , and formulated as:

$$q_{\phi,\eta}(\mathbf{z}|\mathbf{x}) = q_\phi(\mathbf{w}|\mathbf{x}) \left| \frac{\partial f_\eta(\mathbf{w})}{\partial \mathbf{w}} \right|^{-1} \quad (\text{B.1})$$

$$\mathbf{z} = f_\eta(\mathbf{w})$$

where the structure of the RNVP mapping  $f_\eta(\mathbf{w})$  for posterior is exactly the same as  $f_\lambda(\mathbf{z})$  for prior. The ELBO for VAE with RNVP posterior is then simply:

$$\mathcal{L}(\mathbf{x}; \lambda, \theta, \phi, \eta) = \mathbb{E}_{q_\phi(\mathbf{w}|\mathbf{x})} \left[ \log p_\theta(\mathbf{x}|f_\eta(\mathbf{w})) + \log p_\lambda(f_\eta(\mathbf{w})) \right. \\ \left. - \log q_\phi(\mathbf{w}|\mathbf{x}) + \log \left| \det \left( \frac{\partial f_\eta(\mathbf{w})}{\partial \mathbf{w}} \right) \right| \right]$$

### B.3 Additional details of training and evaluation

**General methodology** All the mathematical expressions of expectations *w.r.t.* some distributions are computed by Monte Carlo integration. For example,  $\mathbb{E}_{q_\phi(\mathbf{z}|\mathbf{x})} [f(\mathbf{z}, \mathbf{x})]$  is estimated by:

$$\mathbb{E}_{q_\phi(\mathbf{z}|\mathbf{x})} [f(\mathbf{z}, \mathbf{x})] \approx \frac{1}{L} \sum_{i=1}^L f(\mathbf{z}^{(i)}, \mathbf{x}), \quad \text{where } \mathbf{z}^{(i)} \text{ is one sample from } q_\phi(\mathbf{z}|\mathbf{x})$$

**Training** We use Adam [14] to train our models. The models are trained for 2,400 epochs. The batch size is 128 for DenseVAE, ConvVAE and ResnetVAE, and 64 for PixelVAE. On MNIST, FashionMNIST and Omniglot, we set the learning rate to be  $10^{-3}$  in the first 800 epochs,  $10^{-4}$  in the next 800 epochs, and  $10^{-5}$  in the last 800 epochs. On StaticMNIST, we set the learning rate to be  $10^{-4}$  in the first 1,600 epochs, and  $10^{-5}$  in the last 800 epochs.

L2 regularization with factor  $10^{-4}$  is applied on weights of all non-linear hidden layers, *i.e.*, kernels of non-linear dense layers and convolutional layers, in  $h_\phi(\mathbf{x})$ ,  $h_\theta(\mathbf{z})$ ,  $f_\lambda(\mathbf{z})$  and  $f_\eta(\mathbf{w})$ .

The ELBO is estimated by 1  $\mathbf{z}$  sample for each  $\mathbf{x}$  in training. We adopt warm-up (KL annealing) [3]. The ELBO using warm-up is formulated as:

$$\mathcal{L}(\mathbf{x}; \lambda, \theta, \phi) = \mathbb{E}_{q_\phi(\mathbf{z}|\mathbf{x})} [\log p_\theta(\mathbf{x}|\mathbf{z}) + \beta (\log p_\lambda(\mathbf{z}) - \log q_\phi(\mathbf{z}|\mathbf{x}))]$$

$\beta$  is increased from 0.01 to 1 linearly in the first 100 epochs, and it remains 1 afterwards. The warm-up ELBO for VAEs with Real NVP priors and posteriors can be obtained by replacing  $p_\lambda(\mathbf{z})$  and  $q_\phi(\mathbf{z}|\mathbf{x})$  of the above equation by Eq. (4) and Eq. (B.1), respectively.

We adopt early-stopping using NLL on validation set, to prevent over-fitting on StaticMNIST and PixelVAE. The validation NLL is estimated using 100  $\mathbf{z}$  samples for each  $\mathbf{x}$ , every 20 epochs.

**Training strategies for  $p_\lambda(\mathbf{z})$**  We consider three training strategies for optimizing Eq. (5):

- **Post-hoc training** [1]:  $q_\phi(\mathbf{z}|\mathbf{x})$  and  $p_\theta(\mathbf{x}|\mathbf{z})$  are firstly trained *w.r.t.* the unit Gaussian prior, then  $q_\phi(\mathbf{z}|\mathbf{x})$  and  $p_\theta(\mathbf{x}|\mathbf{z})$  are fixed and  $p_\lambda(\mathbf{z})$  is in turn optimized. This is the most intuitive training method according to Eq. (6), however, it does not work as well as *joint training* in terms of test negative log-likelihood (NLL), which is observed both in our experiments (Table 4) and by Bauer and Mnih [1].
- **Joint training** [35, 1]:  $p_\lambda(\mathbf{z})$  are jointly trained along with  $q_\phi(\mathbf{z}|\mathbf{x})$  and  $p_\theta(\mathbf{x}|\mathbf{z})$ , by directly maximizing Eq. (5).
- **Iterative training**: Proposed by us, we alternate *between* training  $p_\theta(\mathbf{x}|\mathbf{z})$  &  $q_\phi(\mathbf{z}|\mathbf{x})$  and training  $p_\lambda(\mathbf{z})$ , for multiple iterations. The first iteration to train  $p_\theta(\mathbf{x}|\mathbf{z})$  &  $q_\phi(\mathbf{z}|\mathbf{x})$  should use the unit Gaussian prior. Early-stopping should be performed during the whole process if necessary. See Algorithm B.1 for detailed procedure of this strategy. We adopt this method mainly for investigating why *post-hoc training* does not work as well as *joint training*.

---

**Algorithm B.1** Pseudocode for iterative training.

---

**Iteration 1a:** Train  $q_\phi(\mathbf{z}|\mathbf{x})$  and  $p_\theta(\mathbf{x}|\mathbf{z})$ , with  $p_\lambda(\mathbf{z}) = \mathcal{N}(\mathbf{0}, \mathbf{I})$ .  
**Iteration 1b:** Train  $p_\lambda(\mathbf{z})$  for  $2M$  epochs, with fixed  $q_\phi(\mathbf{z}|\mathbf{x})$  and  $p_\theta(\mathbf{x}|\mathbf{z})$ .  
**for**  $i = 2 \dots I$  **do**  
    **Iteration ia:** Train  $q_\phi(\mathbf{z}|\mathbf{x})$  and  $p_\theta(\mathbf{x}|\mathbf{z})$  for  $M$  epochs, with fixed  $p_\lambda(\mathbf{z})$ .  
    **Iteration ib:** Train  $p_\lambda(\mathbf{z})$  for  $M$  epochs, with fixed  $q_\phi(\mathbf{z}|\mathbf{x})$  and  $p_\theta(\mathbf{x}|\mathbf{z})$ .  
**end for**

---

To train  $p_\lambda(\mathbf{z})$  with *post-hoc* strategy, we start from a trained VAE, adding RNVP prior onto it, and optimizing the Real NVP  $f_\lambda(\mathbf{z})$  for 3,200 epochs, with learning rate set to  $10^{-3}$  in the first 1,600 epochs, and  $10^{-4}$  in the final 1,600 epochs.

Algorithm B.1 is the pseudocode of *iterative training* strategy. For Iteration 1a, all hyper-parameters are the same with training a standard VAE, where in particular, the training epoch is set to 2,400. For Iteration 1b, the learning rate is  $10^{-3}$  for the first  $M$  epochs, and is  $10^{-4}$  for the next  $M$  epochs. For all the next iterations, learning rate is always  $10^{-4}$ . The number of iterations  $I$  is chosen to be 16, and the number of epochs  $M$  is chosen to be 100, for MNIST, FashionMNIST and Omniglot. For StaticMNIST, we find it overfits after only a few iterations, thus we choose  $I$  to be 4, and  $M$  to be 400. With these hyper-parameters,  $q_\phi(\mathbf{z}|\mathbf{x})$ ,  $p_\theta(\mathbf{x}|\mathbf{z})$  and  $p_\lambda(\mathbf{z})$  are *iteratively trained* for totally 3,200 epochs on all datasets (starting from Iteration 1b), after the pre-training step (Iteration 1a).

**Regularization term for  $q_\phi(\mathbf{z})$**  In order to compare some metrics (*e.g.*, the *active units*) of VAE with RNVP prior to those of standard VAE, we introduce an additional regularization term for  $q_\phi(\mathbf{z})$ , such that  $q_\phi(\mathbf{z})$  of VAE using RNVP prior would have roughly zero mean and unit variance, just as a standard VAE with unit Gaussian prior. The regularization term for  $q_\phi(\mathbf{z})$  (denoted as  $\text{Reg}[q_\phi(\mathbf{z})]$ ) and the final training objective augmented with the regularization term (denoted as  $\tilde{\mathcal{L}}(\mathbf{x}; \lambda, \theta, \phi)$ ) is:

$$\text{Reg}[q_\phi(\mathbf{z})] = \frac{1}{\text{Dim}(\mathbf{z})} \sum_{k=1}^{\text{Dim}(\mathbf{z})} \left[ (\text{Mean}[z_k])^2 + (\text{Var}[z_k] - 1)^2 \right]$$
$$\tilde{\mathcal{L}}(\lambda, \theta, \phi) = \mathbb{E}_{p^*(\mathbf{x})} \mathcal{L}(\mathbf{x}; \lambda, \theta, \phi) + \text{Reg}[q_\phi(\mathbf{z})]$$

where  $z_k$  is the  $k$ -th dimension of  $\mathbf{z}$ ,  $\text{Dim}(\mathbf{z})$  is the number of dimensions,  $\text{Mean}[z_k] = \mathbb{E}_{p^*(\mathbf{x})} \mathbb{E}_{q_\phi(\mathbf{z}|\mathbf{x})} [z_k]$  and  $\text{Var}[z_k] = \mathbb{E}_{p^*(\mathbf{x})} \mathbb{E}_{q_\phi(\mathbf{z}|\mathbf{x})} \left[ (z_k - \text{Mean}[z_k])^2 \right]$  are the mean and variance of each dimension.

Table B.1: Avg.  $\text{Mean}[z_k]$  and  $\text{Var}[z_k]$  of regularized/un-regularized ResnetVAE with RNVP prior.

Datasets	regularized		un-regularized	
	Avg. $\text{Mean}[z_k]$	Avg. $\text{Var}[z_k]$	Avg. $\text{Mean}[z_k]$	Avg. $\text{Var}[z_k]$
StaticMNIST	$-0.02 \pm 0.03$	$0.93 \pm 0.01$	$0.05 \pm 0.37$	$1.50 \pm 0.02$
MNIST	$0.00 \pm 0.00$	$0.98 \pm 0.01$	$-0.06 \pm 0.02$	$0.76 \pm 0.04$
FashionMNIST	$0.00 \pm 0.00$	$0.98 \pm 0.00$	$0.00 \pm 0.03$	$0.86 \pm 0.07$
Omniglot	$0.00 \pm 0.02$	$0.95 \pm 0.00$	$0.00 \pm 0.01$	$0.24 \pm 0.01$

Table B.1 shows the average  $\text{Mean}[z_k]$  and  $\text{Var}[z_k]$  of ResnetVAE with RNVP prior, computed on test data. Average  $\text{Mean}[z_k]$  is defined as  $\frac{1}{\text{Dim}(\mathbf{z})} \sum_{k=1}^{\text{Dim}(\mathbf{z})} \text{Mean}[z_k]$ , while average  $\text{Var}[z_k]$  is defined as  $\frac{1}{\text{Dim}(\mathbf{z})} \sum_{k=1}^{\text{Dim}(\mathbf{z})} \text{Var}[z_k]$ . The means and standard deviations of the above table is computed *w.r.t.* repeated experiments. Using the regularization term for  $q_\phi(\mathbf{z})$  makes the  $\text{Mean}[z_k]$  and  $\text{Var}[z_k]$  of  $\mathbf{z}$  samples close to  $\mathcal{N}(\mathbf{0}, \mathbf{I})$ , which is in sharp contrast with the un-regularized case. For fair comparison in Table 8 and Fig. 3, it is crucial to have  $\text{Mean}[z_k]$  and  $\text{Var}[z_k]$  close to  $\mathcal{N}(\mathbf{0}, \mathbf{I})$ . Test NLLs are not reported here, because we find no significant difference between regularized and un-regularized models in terms of test NLLs.

**Evaluation** The *negative log-likelihood* (NLL), the *reconstruction loss* and the KL divergence  $\mathbb{E}_{p^*(\mathbf{x})} \text{D}_{KL}[q_\phi(\mathbf{z}|\mathbf{x}) \| p_\lambda(\mathbf{z})]$  are estimated with 1000  $\mathbf{z}$  samples from  $q_\phi(\mathbf{z}|\mathbf{x}^{(i)})$  for each  $\mathbf{x}^{(i)}$  from

test data:

$$\text{NLL} \approx \frac{1}{N} \sum_{i=1}^N \text{LogMeanExp}_{j=1}^{1000} \left[ \log p_{\theta}(\mathbf{x}^{(i)} | \mathbf{z}^{(i,j)}) + \log p_{\lambda}(\mathbf{z}^{(i,j)}) - \log q_{\phi}(\mathbf{z}^{(i,j)} | \mathbf{x}^{(i)}) \right]$$

$$\text{Reconstruction Loss} \approx \frac{1}{1000N} \sum_{i=1}^N \sum_{j=1}^{1000} \left[ \log p_{\theta}(\mathbf{x}^{(i)} | \mathbf{z}^{(i,j)}) \right]$$

$$\mathbb{E}_{p^*(\mathbf{x})} \text{D}_{KL}[q_{\phi}(\mathbf{z} | \mathbf{x}) \| p_{\lambda}(\mathbf{z})] \approx \frac{1}{1000N} \sum_{i=1}^N \sum_{j=1}^{1000} \left[ \log q_{\phi}(\mathbf{z}^{(i,j)} | \mathbf{x}^{(i)}) - \log p_{\lambda}(\mathbf{z}^{(i,j)}) \right]$$

where each  $\mathbf{z}^{(i,j)}$  is one sample from  $q_{\phi}(\mathbf{z} | \mathbf{x}^{(i)})$ , and  $\text{LogMeanExp}_{j=1}^L [f(\mathbf{x}^{(i)}, \mathbf{z}^{(i,j)})]$  is:

$$\begin{aligned} \text{LogMeanExp}_{j=1}^L [f(\mathbf{x}^{(i)}, \mathbf{z}^{(i,j)})] &= f_{max} + \log \frac{1}{L} \sum_{j=1}^L \left[ \exp(f(\mathbf{x}^{(i)}, \mathbf{z}^{(i,j)}) - f_{max}) \right] \\ f_{max} &= \max_j f(\mathbf{x}^{(i)}, \mathbf{z}^{(i,j)}) \end{aligned}$$

**Active units** *active units* [4] is defined as the number of latent dimensions whose variance is larger than 0.01. The variance of the  $k$ -th dimension is formulated as:

$$\text{Var}_k = \text{Var}_{p^*(\mathbf{x})} [\mathbb{E}_{q_{\phi}(\mathbf{z} | \mathbf{x})} [z_k]]$$

where  $z_k$  is the  $k$ -th dimension of  $\mathbf{z}$ . We compute  $\text{Var}_k$  on the training data, while the inner expectation  $\mathbb{E}_{q_{\phi}(\mathbf{z} | \mathbf{x})} [z_k]$  is estimated by drawing 1,000 samples of  $\mathbf{z}$  for each  $\mathbf{x}$ .

#### B.4 Formulation of closest pairs of $q_{\phi}(\mathbf{z} | \mathbf{x})$ and others

**Closest pairs of  $q_{\phi}(\mathbf{z} | \mathbf{x})$**  For each  $\mathbf{x}^{(i)}$  from training data, we find the training point  $\mathbf{x}^{(j)}$ , whose posterior  $q_{\phi}(\mathbf{z} | \mathbf{x}^{(j)})$  is the closest neighbor to  $q_{\phi}(\mathbf{z} | \mathbf{x}^{(i)})$ :

$$j = \arg \min_{j \neq i} \|\boldsymbol{\mu}_{\phi}(\mathbf{x}^{(j)}) - \boldsymbol{\mu}_{\phi}(\mathbf{x}^{(i)})\|$$

where  $\boldsymbol{\mu}_{\phi}(\mathbf{x})$  is the mean of  $q_{\phi}(\mathbf{z} | \mathbf{x})$ , and  $\|\cdot\|$  is the L2 norm. These two posteriors  $q_{\phi}(\mathbf{z} | \mathbf{x}^{(i)})$  and  $q_{\phi}(\mathbf{z} | \mathbf{x}^{(j)})$  are called a closest pair of  $q_{\phi}(\mathbf{z} | \mathbf{x})$ .

**Distance of a pair of  $q_{\phi}(\mathbf{z} | \mathbf{x})$**  The distance  $d_{ij}$  of a closest pair  $q_{\phi}(\mathbf{z} | \mathbf{x}^{(i)})$  and  $q_{\phi}(\mathbf{z} | \mathbf{x}^{(j)})$  is:

$$\begin{aligned} \mathbf{d}_{ij} &= \boldsymbol{\mu}_{\phi}(\mathbf{x}^{(j)}) - \boldsymbol{\mu}_{\phi}(\mathbf{x}^{(i)}) \\ d_{ij} &= \|\mathbf{d}_{ij}\| \end{aligned}$$

**Normalized distance of a pair of  $q_{\phi}(\mathbf{z} | \mathbf{x})$**  For each closest pair  $q_{\phi}(\mathbf{z} | \mathbf{x}^{(i)})$  and  $q_{\phi}(\mathbf{z} | \mathbf{x}^{(j)})$ , we compute its *normalized distance*  $\widetilde{d}_{ij}$  by:

$$\widetilde{d}_{ij} = \frac{2d_{ij}}{\text{Std}[i; j] + \text{Std}[j; i]} \quad (\text{B.2})$$

$\text{Std}[i; j]$  is formulated as:

$$\text{Std}[i; j] = \sqrt{\text{Var}_{q_{\phi}(\mathbf{z} | \mathbf{x}^{(i)})} \left[ (\mathbf{z} - \boldsymbol{\mu}_{\phi}(\mathbf{x}^{(i)})) \cdot \frac{\mathbf{d}_{ij}}{d_{ij}} \right]} \quad (\text{B.3})$$

where  $\text{Var}_{q_{\phi}(\mathbf{z} | \mathbf{x}^{(i)})} [f(\mathbf{z})]$  is the variance of  $f(\mathbf{z})$  w.r.t.  $q_{\phi}(\mathbf{z} | \mathbf{x}^{(i)})$ . We use 1,000 samples to estimate each  $\text{Std}[i; j]$ . Roughly speaking, the *normalized distance*  $\widetilde{d}_{ij}$  can be viewed as “distance/std” along the direction of  $\mathbf{d}_{ij}$ , which indicates the scale of the “hole” between  $q_{\phi}(\mathbf{z} | \mathbf{x}^{(i)})$  and  $q_{\phi}(\mathbf{z} | \mathbf{x}^{(j)})$ .

### B.5 Discussions about $D_{KL}[q_\phi(\mathbf{z})||p_\lambda(\mathbf{z})]$

The KL divergence between the *aggregated posterior* and the prior, *i.e.*,  $D_{KL}[q_\phi(\mathbf{z})||p_\lambda(\mathbf{z})]$ , is first analyzed by Hoffman and Johnson [11] as one component of the ELBO decomposition (6). Since  $q_\phi(\mathbf{z}) = \int q_\phi(\mathbf{z}|\mathbf{x}) p^*(\mathbf{x}) d\mathbf{x}$  and  $p_\lambda(\mathbf{z}) = \int p_\theta(\mathbf{z}|\mathbf{x}) p_\theta(\mathbf{x}) d\mathbf{x}$ , Rosca et al. [28] used this KL divergence as a metric to quantify the approximation quality of both  $p_\theta(\mathbf{x})$  to  $p^*(\mathbf{x})$ , and  $q_\phi(\mathbf{z}|\mathbf{x})$  to  $p_\theta(\mathbf{z}|\mathbf{x})$ . As we are focusing on learning the prior,  $D_{KL}[q_\phi(\mathbf{z})||p_\lambda(\mathbf{z})]$  can in turn be a metric for quantifying whether  $p_\lambda(\mathbf{z})$  is close enough to the *aggregated posterior*  $q_\phi(\mathbf{z})$ .

The evaluation of  $D_{KL}[q_\phi(\mathbf{z})||p_\lambda(\mathbf{z})]$ , however, is not an easy task. One way to estimate the KL divergence of two arbitrary distributions is the density ratio trick [33, 22], where  $D_{KL}[q_\phi(\mathbf{z})||p_\lambda(\mathbf{z})]$  is estimated by a separately trained neural network classifier. However, Rosca et al. [28] revealed that such approach can under-estimate  $D_{KL}[q_\phi(\mathbf{z})||p_\lambda(\mathbf{z})]$ , and the training may even diverge when  $\mathbf{z}$  has hundreds of or more dimensions.

Another approach is to directly estimate  $D_{KL}[q_\phi(\mathbf{z})||p_\lambda(\mathbf{z})]$  by Monte Carlo integration. The KL divergence can be rewritten into the following form:

$$\begin{aligned} D_{KL}[q_\phi(\mathbf{z})||p_\lambda(\mathbf{z})] &= \int q_\phi(\mathbf{z}) \log \frac{q_\phi(\mathbf{z})}{p_\lambda(\mathbf{z})} d\mathbf{z} \\ &= \int \left( \int q_\phi(\mathbf{z}|\mathbf{x}) p^*(\mathbf{x}) d\mathbf{x} \right) \log \frac{\int q_\phi(\mathbf{z}|\mathbf{x}') p^*(\mathbf{x}') d\mathbf{x}'}{p_\lambda(\mathbf{z})} d\mathbf{z} \\ &= \int p^*(\mathbf{x}) \int q_\phi(\mathbf{z}|\mathbf{x}) \log \frac{\int q_\phi(\mathbf{z}|\mathbf{x}') p^*(\mathbf{x}') d\mathbf{x}'}{p_\lambda(\mathbf{z})} d\mathbf{z} d\mathbf{x} \\ &= \mathbb{E}_{p^*(\mathbf{x})} \mathbb{E}_{q_\phi(\mathbf{z}|\mathbf{x})} [\log \mathbb{E}_{p^*(\mathbf{x}')} [q_\phi(\mathbf{z}|\mathbf{x}')] - \log p_\lambda(\mathbf{z})] \end{aligned} \quad (\text{B.4})$$

Rosca et al. [28] has already proposed a Monte Carlo based algorithm to estimate  $D_{KL}[q_\phi(\mathbf{z})||p_\lambda(\mathbf{z})]$ , in case that the training data is statically binarized. Since we mainly use dynamically binarized datasets, we slightly modified the algorithm according to Eq. (B.4), to allow sampling multiple  $\mathbf{x}$  from each image. Our algorithm is:

---

**Algorithm B.2** Pseudocode for estimating  $D_{KL}[q_\phi(\mathbf{z})||p_\lambda(\mathbf{z})]$  (denoted as `marginal_kl`) on dynamically binarized dataset, where  $\mu$  is the pixel intensities of each original image.

---

```

x_samples = []
for  $\mu$  in training dataset do
    for  $i = 1 \dots n_x$  do
        sample  $\mathbf{x}$  from Bernoulli( $\mu$ )
        append  $\mathbf{x}$  to x_samples
    end for
end for
marginal_kl = 0
for  $\mathbf{x}$  in x_samples do
    for  $i = 1 \dots n_z$  do
        sample  $\mathbf{z}$  from  $q_\phi(\mathbf{z}|\mathbf{x})$ 
        posterior_list = []
        for  $\mathbf{x}'$  in x_samples do
            append  $\log q_\phi(\mathbf{z}|\mathbf{x}')$  to posterior_list
        end for
         $\log q_\phi(\mathbf{z}) = \text{LogMeanExp}(\text{posterior\_list})$ 
         $\text{marginal\_kl} = \text{marginal\_kl} + \log q_\phi(\mathbf{z}) - \log p_\lambda(\mathbf{z})$ 
    end for
end for
marginal_kl = marginal_kl / (len(x_samples)  $\times$   $n_z$ )

```

---

Surprisingly, we find that increasing  $n_x$  will cause the estimated  $D_{KL}[q_\phi(\mathbf{z})||p_\lambda(\mathbf{z})]$  to decrease on MNIST, see Table B.2. Given that our  $n_z = 10$  for all  $n_x$ , the number of our sampled  $\mathbf{z}$  (even when  $n_x = 1$ ) is  $10 \times 60,000 = 6 \times 10^5$ , which should not be too small, since Rosca et al. [28] only used  $10^6$   $\mathbf{z}$  in their experiments. When  $n_x = 8$ , the number of  $\mathbf{z}$  is  $8 \times 10 \times 60,000 = 4.8 \times 10^6$ , which is

4.8x larger than Rosca et al. [28], not to mention the inner expectation  $\mathbb{E}_{p^*(\mathbf{x}')} [q_\phi(\mathbf{z}|\mathbf{x}')]$  is estimated with 8x larger number of  $\mathbf{x}'$ . There should be in total 38.4x larger number of  $\log q_\phi(\mathbf{z}|\mathbf{x}')$  computed for estimating  $D_{KL}[q_\phi(\mathbf{z})||p_\lambda(\mathbf{z})]$  than Rosca et al. [28], which has already costed about 3 days on 4 GTX 1080 Ti graphical cards. We believe such a large number of Monte Carlo samples should be sufficient for any well-defined algorithm.

Table B.2:  $D_{KL}[q_\phi(\mathbf{z})||p_\lambda(\mathbf{z})]$  of a ResnetVAE with RNVP prior trained on MNIST, estimated by Algorithm B.2.  $n_z = 10$  for all  $n_x$ . We only tried  $n_x$  for up to 8, due to the growing computation time of  $O(n_x^2)$ .

$n_x$	1	2	3	5	8
$D_{KL}[q_\phi(\mathbf{z})  p_\lambda(\mathbf{z})]$	15.279	14.623	14.254	13.796	13.392

According to the above observation, we suspect there must be some flaw in Algorithm B.2. Because of this, we do not adopt Algorithm B.2 to estimate  $D_{KL}[q_\phi(\mathbf{z})||p_\lambda(\mathbf{z})]$ .

Since no mature method has been published to estimate  $D_{KL}[q_\phi(\mathbf{z})||p_\lambda(\mathbf{z})]$  yet, we decide not to use  $D_{KL}[q_\phi(\mathbf{z})||p_\lambda(\mathbf{z})]$  to measure how our learned  $p_\lambda(\mathbf{z})$  approximates the *aggregated posterior*  $q_\phi(\mathbf{z})$ .

## B.6 Additional quantitative results

Table B.3: Test NLL of different models, with both prior and posterior being Gaussian (“standard”), only posterior being Real NVP (“RNVP  $q(z|x)$ ”), and only prior being Real NVP (“RNVP  $p(z)$ ”). Flow depth  $K = 20$ .

Models		Datasets			
		StaticMNIST	MNIST	FashionMNIST	Omniglot
DenseVAE	standard	88.84 $\pm$ 0.05	84.48 $\pm$ 0.03	228.60 $\pm$ 0.03	106.42 $\pm$ 0.14
	RNVP $q(z x)$	86.07 $\pm$ 0.11	82.53 $\pm$ 0.00	227.79 $\pm$ 0.01	102.97 $\pm$ 0.06
	RNVP $p(z)$	<b>84.87 <math>\pm</math> 0.05</b>	<b>80.43 <math>\pm</math> 0.01</b>	<b>226.11 <math>\pm</math> 0.02</b>	<b>102.19 <math>\pm</math> 0.12</b>
ConvVAE	standard	83.63 $\pm$ 0.01	82.14 $\pm$ 0.01	227.51 $\pm$ 0.08	97.87 $\pm$ 0.02
	RNVP $q(z x)$	81.11 $\pm$ 0.03	80.09 $\pm$ 0.01	226.03 $\pm$ 0.00	94.90 $\pm$ 0.03
	RNVP $p(z)$	<b>80.06 <math>\pm</math> 0.07</b>	<b>78.67 <math>\pm</math> 0.01</b>	<b>224.65 <math>\pm</math> 0.01</b>	<b>93.68 <math>\pm</math> 0.01</b>
ResnetVAE	standard	82.95 $\pm$ 0.09	81.07 $\pm$ 0.03	226.17 $\pm$ 0.05	96.99 $\pm$ 0.04
	RNVP $q(z x)$	80.97 $\pm$ 0.05	79.53 $\pm$ 0.03	225.02 $\pm$ 0.01	94.30 $\pm$ 0.02
	RNVP $p(z)$	<b>79.99 <math>\pm</math> 0.02</b>	<b>78.58 <math>\pm</math> 0.01</b>	<b>224.09 <math>\pm</math> 0.01</b>	<b>93.61 <math>\pm</math> 0.04</b>
PixelVAE	standard	79.47 $\pm$ 0.02	78.64 $\pm$ 0.02	224.22 $\pm$ 0.06	89.83 $\pm$ 0.04
	RNVP $q(z x)$	79.09 $\pm$ 0.01	78.41 $\pm$ 0.01	223.81 $\pm$ 0.00	89.69 $\pm$ 0.01
	RNVP $p(z)$	<b>78.92 <math>\pm</math> 0.02</b>	<b>78.15 <math>\pm</math> 0.04</b>	<b>223.40 <math>\pm</math> 0.07</b>	<b>89.61 <math>\pm</math> 0.03</b>

Table B.4: Test NLL of ResnetVAE, with only Real NVP posterior (“RNVP  $q(z|x)$ ”), only Real NVP prior (“RNVP  $p(z)$ ”), and both Real NVP prior & posterior (“both”). Flow depth  $K = 20$ .

Datasets	ResnetVAE		
	RNVP $q(z x)$	RNVP $p(z)$	both
StaticMNIST	80.97 $\pm$ 0.05	79.99 $\pm$ 0.02	<b>79.87 <math>\pm</math> 0.04</b>
MNIST	79.53 $\pm$ 0.03	78.58 $\pm$ 0.01	<b>78.56 <math>\pm</math> 0.01</b>
FashionMNIST	225.02 $\pm$ 0.01	224.09 $\pm$ 0.01	<b>224.08 <math>\pm</math> 0.02</b>
Omniglot	94.30 $\pm$ 0.02	<b>93.61 <math>\pm</math> 0.04</b>	93.68 $\pm$ 0.04

Table B.5: Test NLL of ResnetVAE, with Real NVP prior of different flow depth.

Flow depth	Datasets			
	StaticMNIST	MNIST	FashionMNIST	Omniglot
0	82.95 $\pm$ 0.09	81.07 $\pm$ 0.03	226.17 $\pm$ 0.05	96.99 $\pm$ 0.04
1	81.76 $\pm$ 0.04	80.02 $\pm$ 0.02	225.27 $\pm$ 0.03	96.20 $\pm$ 0.06
2	81.30 $\pm$ 0.02	79.58 $\pm$ 0.02	224.78 $\pm$ 0.02	95.35 $\pm$ 0.06
5	80.64 $\pm$ 0.06	79.09 $\pm$ 0.02	224.37 $\pm$ 0.01	94.47 $\pm$ 0.01
10	80.26 $\pm$ 0.05	78.75 $\pm$ 0.01	224.18 $\pm$ 0.01	93.92 $\pm$ 0.02
20	79.99 $\pm$ 0.02	78.58 $\pm$ 0.01	224.09 $\pm$ 0.01	93.61 $\pm$ 0.04
30	79.90 $\pm$ 0.05	78.52 $\pm$ 0.01	<b>224.07 <math>\pm</math> 0.01</b>	93.53 $\pm$ 0.02
50	<b>79.84 <math>\pm</math> 0.04</b>	<b>78.49 <math>\pm</math> 0.01</b>	<b>224.07 <math>\pm</math> 0.01</b>	<b>93.52 <math>\pm</math> 0.02</b>

Table B.6: Test NLL on StaticMNIST. “ $\dagger$ ” and “ $\ddagger$ ” has the same meaning as Table 5.

Model	NLL
<i>Models without PixelCNN decoder</i>	
ConvHVAE + Lars prior $\dagger$ [1]	81.70
ConvHVAE + VampPrior $\dagger$ [35]	81.09
VAE + IAF $\ddagger$ [16]	79.88
BIVA $\ddagger$ [20]	<b>78.59</b>
Our ConvVAE + RNVP $p(z)$ , $K = 50$	80.09 $\pm$ 0.01
Our ResnetVAE + RNVP $p(z)$ , $K = 50$	79.84 $\pm$ 0.04
<i>Models with PixelCNN decoder</i>	
VLAE $\ddagger$ [5]	79.03
PixelHVAE + VampPrior $\dagger$ [35]	79.78
Our PixelVAE + RNVP $p(z)$ , $K = 50$	<b>79.01 <math>\pm</math> 0.03</b>

Table B.7: Test NLL on MNIST. “ $\dagger$ ” and “ $\ddagger$ ” has the same meaning as Table 5.

Model	NLL
<i>Models without PixelCNN decoder</i>	
ConvHVAE + Lars prior $\dagger$ [1]	80.30
ConvHVAE + VampPrior $\dagger$ [35]	79.75
VAE + IAF $\ddagger$ [16]	79.10 $\pm$ 0.07
BIVA $\ddagger$ [20]	<b>78.41</b>
Our ConvVAE + RNVP $p(z)$ , $K = 50$	78.61 $\pm$ 0.01
Our ResnetVAE + RNVP $p(z)$ , $K = 50$	78.49 $\pm$ 0.01
<i>Models with PixelCNN decoder</i>	
VLAE $\ddagger$ [5]	78.53
PixelVAE $\ddagger$ [10]	79.02
PixelHVAE + VampPrior $\dagger$ [35]	78.45
Our PixelVAE + RNVP $p(z)$ , $K = 50$	<b>78.12 <math>\pm</math> 0.04</b>

Table B.8: Test NLL on Omniglot. “ $\dagger$ ” and “ $\ddagger$ ” has the same meaning as Table 5.

Model	NLL
<i>Models without PixelCNN decoder</i>	
ConvHVAE + Lars prior $\dagger$ [1]	97.08
ConvHVAE + VampPrior $\dagger$ [35]	97.56
BIVA $\ddagger$ [20]	<b>91.34</b>
Our ConvVAE + RNVP $p(z)$ , $K = 50$	93.62 $\pm$ 0.02
Our ResnetVAE + RNVP $p(z)$ , $K = 50$	93.52 $\pm$ 0.02
<i>Models with PixelCNN decoder</i>	
VLAE $\ddagger$ [5]	89.83
PixelHVAE + VampPrior $\dagger$ [35]	89.76
Our PixelVAE + RNVP $p(z)$ , $K = 50$	<b>89.60 <math>\pm</math> 0.01</b>

Table B.9: Test NLL on FashionMNIST. “ $\dagger$ ” and “ $\ddagger$ ” has the same meaning as Table 5.

Model	NLL
<i>Models without PixelCNN decoder</i>	
ConvHVAE + Lars prior $^\dagger$ [1]	225.92
<i>Our ConvVAE + RNVP <math>p(z)</math>, <math>K = 50</math></i>	$224.64 \pm 0.01$
<i>Our ResnetVAE + RNVP <math>p(z)</math>, <math>K = 50</math></i>	<b><math>224.07 \pm 0.01</math></b>
<i>Models with PixelCNN decoder</i>	
<i>Our PixelVAE + RNVP <math>p(z)</math>, <math>K = 50</math></i>	<b><math>223.36 \pm 0.06</math></b>

Table B.10: Test NLL of ResnetVAE, with prior trained by: *joint* training, *iterative* training, *post-hoc* training, and standard VAE (“none”) as reference. Flow depth  $K = 20$ .

Datasets	ResnetVAE			
	joint	iterative	post-hoc	none
StaticMNIST	<b><math>79.99 \pm 0.02</math></b>	$80.63 \pm 0.02$	$80.86 \pm 0.04$	$82.95 \pm 0.09$
MNIST	<b><math>78.58 \pm 0.01</math></b>	$79.61 \pm 0.01$	$79.90 \pm 0.04$	$81.07 \pm 0.03$
FashionMNIST	<b><math>224.09 \pm 0.01</math></b>	$224.88 \pm 0.02$	$225.22 \pm 0.01$	$226.17 \pm 0.05$
Omniglot	<b><math>93.61 \pm 0.04</math></b>	$94.43 \pm 0.11$	$94.87 \pm 0.05$	$96.99 \pm 0.04$



## B.7 Additional qualitative results

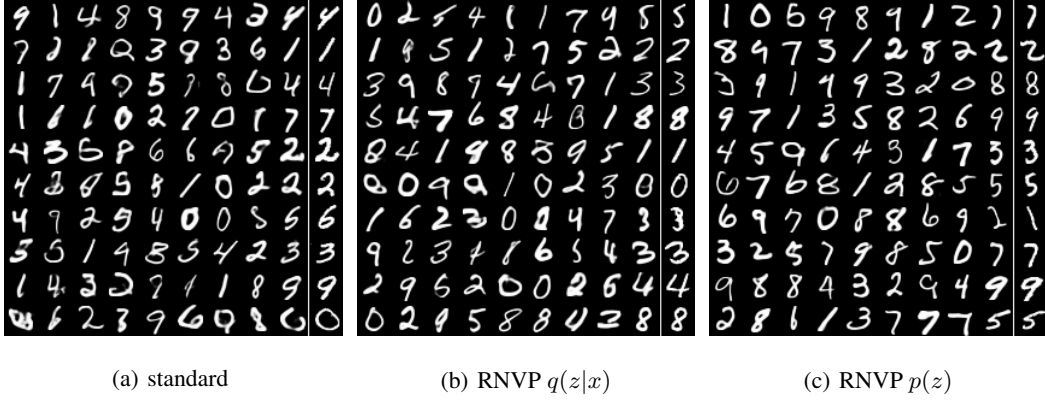


Figure B.1: Samples from ResnetVAE trained on MNIST. The last column of each 10x10 grid show the images from the training set, most similar to the second-to-last column in pixel-wise L2 distance.

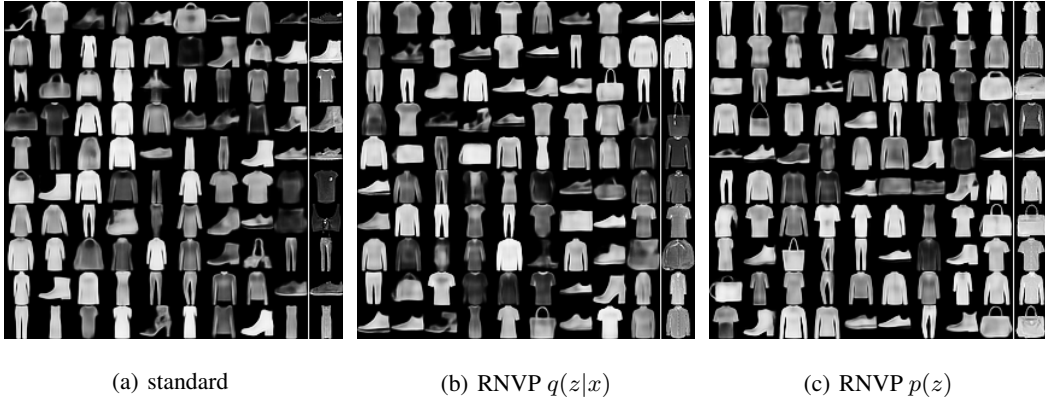


Figure B.2: Samples from ResnetVAE trained on FashionMNIST. The last column of each 10x10 grid show the images from the training set, most similar to the second-to-last column in pixel-wise L2 distance.

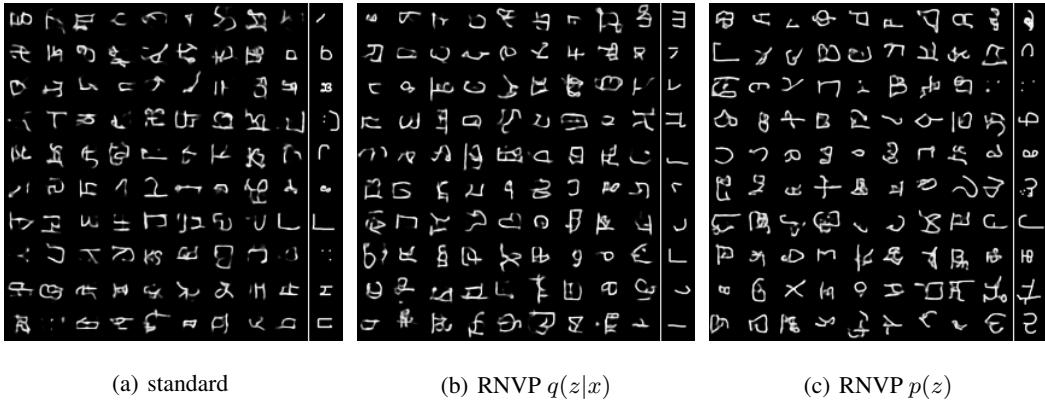


Figure B.3: Samples from ResnetVAE trained on Omniglot. The last column of each 10x10 grid show the images from the training set, most similar to the second-to-last column in pixel-wise L2 distance.

### B.8 Additional results: improved reconstruction loss and other experimental results with learned prior

Table B.11: Average test *elbo*, *reconstruction loss* (“*recons*”),  $\mathbb{E}_{p^*(\mathbf{x})} D_{KL}[q_\phi(\mathbf{z}|\mathbf{x})\|p_\lambda(\mathbf{z})]$  (“*kl*”) and  $\mathbb{E}_{p^*(\mathbf{x})} D_{KL}[q_\phi(\mathbf{z}|\mathbf{x})\|p_\theta(\mathbf{z}|\mathbf{x})]$  (“*kl<sub>z|x</sub>*”) of various DenseVAE. Flow depth  $K = 20$ .

Datasets	standard			
	<i>elbo</i>	<i>recons</i>	<i>kl</i>	<i>kl<sub>z x</sub></i>
StaticMNIST	-94.53	-65.54	29.00	5.69
MNIST	-88.19	-62.04	<b>26.16</b>	3.71
FashionMNIST	-230.81	-211.71	<b>19.11</b>	2.22
Omniglot	-113.59	-78.25	35.33	7.17

Datasets	RNVP $q(z x)$			
	<i>elbo</i>	<i>recons</i>	<i>kl</i>	<i>kl<sub>z x</sub></i>
StaticMNIST	-90.78	<b>-62.55</b>	28.23	4.71
MNIST	-85.15	-58.83	26.31	2.62
FashionMNIST	-229.53	-210.35	19.18	1.75
Omniglot	-108.54	-73.71	<b>34.83</b>	<b>5.57</b>

Datasets	RNVP $p(z)$			
	<i>elbo</i>	<i>recons</i>	<i>kl</i>	<i>kl<sub>z x</sub></i>
StaticMNIST	<b>-88.87</b>	-63.35	<b>25.52</b>	<b>4.00</b>
MNIST	<b>-82.57</b>	<b>-55.99</b>	26.58	<b>2.14</b>
FashionMNIST	<b>-227.72</b>	<b>-208.13</b>	19.59	<b>1.61</b>
Omniglot	<b>-107.99</b>	<b>-73.10</b>	34.89	5.80

Table B.12: Average test *elbo*, *reconstruction loss* (“*recons*”),  $\mathbb{E}_{p^*(\mathbf{x})} D_{KL}[q_\phi(\mathbf{z}|\mathbf{x})\|p_\lambda(\mathbf{z})]$  (“*kl*”) and  $\mathbb{E}_{p^*(\mathbf{x})} D_{KL}[q_\phi(\mathbf{z}|\mathbf{x})\|p_\theta(\mathbf{z}|\mathbf{x})]$  (“*kl<sub>z|x</sub>*”) of various ConvVAE. Flow depth  $K = 20$ .

Datasets	standard			
	<i>elbo</i>	<i>recons</i>	<i>kl</i>	<i>kl<sub>z x</sub></i>
StaticMNIST	-88.15	-60.34	27.81	4.51
MNIST	-85.89	-58.97	26.92	3.75
FashionMNIST	-230.43	-210.24	<b>20.18</b>	2.92
Omniglot	-104.70	-66.00	38.70	6.83

Datasets	RNVP $q(z x)$			
	<i>elbo</i>	<i>recons</i>	<i>kl</i>	<i>kl<sub>z x</sub></i>
StaticMNIST	-83.92	-56.67	<b>27.25</b>	<b>2.82</b>
MNIST	-82.46	-56.08	<b>26.38</b>	2.37
FashionMNIST	-228.20	-207.33	20.88	2.18
Omniglot	-99.92	-62.48	<b>37.44</b>	5.02

Datasets	RNVP $p(z)$			
	<i>elbo</i>	<i>recons</i>	<i>kl</i>	<i>kl<sub>z x</sub></i>
StaticMNIST	<b>-82.91</b>	<b>-54.01</b>	28.90	2.86
MNIST	<b>-80.42</b>	<b>-53.33</b>	27.09	<b>1.75</b>
FashionMNIST	<b>-226.65</b>	<b>-204.93</b>	21.72	<b>2.00</b>
Omniglot	<b>-98.59</b>	<b>-59.07</b>	39.51	<b>4.91</b>

Table B.13: Average test *elbo*, *reconstruction loss* (“*recons*”),  $\mathbb{E}_{p^*(\mathbf{x})} D_{KL}[q_\phi(\mathbf{z}|\mathbf{x})||p_\lambda(\mathbf{z})]$  (“*kl*”) and  $\mathbb{E}_{p^*(\mathbf{x})} D_{KL}[q_\phi(\mathbf{z}|\mathbf{x})||p_\theta(\mathbf{z}|\mathbf{x})]$  (“*kl<sub>z|x</sub>*”) of various ResnetVAE. Flow depth  $K = 20$ .

Datasets	standard			
	<i>elbo</i>	<i>recons</i>	<i>kl</i>	<i>kl<sub>z x</sub></i>
StaticMNIST	-87.61	-60.09	27.52	4.67
MNIST	-84.62	-58.70	25.92	3.55
FashionMNIST	-228.91	-208.94	<b>19.96</b>	2.74
Omniglot	-104.87	-66.98	37.89	7.88
Datasets	RNVP $q(z x)$			
	<i>elbo</i>	<i>recons</i>	<i>kl</i>	<i>kl<sub>z x</sub></i>
StaticMNIST	-84.72	-58.10	<b>26.63</b>	3.75
MNIST	-81.95	-56.15	<b>25.80</b>	2.42
FashionMNIST	-227.16	-206.61	20.54	2.14
Omniglot	-100.30	-63.34	<b>36.96</b>	6.00
Datasets	RNVP $p(z)$			
	<i>elbo</i>	<i>recons</i>	<i>kl</i>	<i>kl<sub>z x</sub></i>
StaticMNIST	<b>-82.85</b>	<b>-54.32</b>	28.54	<b>2.87</b>
MNIST	<b>-80.34</b>	<b>-53.64</b>	26.70	<b>1.76</b>
FashionMNIST	<b>-225.97</b>	<b>-204.66</b>	21.31	<b>1.88</b>
Omniglot	<b>-99.60</b>	<b>-61.21</b>	38.39	<b>5.99</b>

Table B.14: Average test *elbo*, *reconstruction loss* (“*recons*”),  $\mathbb{E}_{p^*(\mathbf{x})} D_{KL}[q_\phi(\mathbf{z}|\mathbf{x})||p_\lambda(\mathbf{z})]$  (“*kl*”) and  $\mathbb{E}_{p^*(\mathbf{x})} D_{KL}[q_\phi(\mathbf{z}|\mathbf{x})||p_\theta(\mathbf{z}|\mathbf{x})]$  (“*kl<sub>z|x</sub>*”) of various PixelVAE. Flow depth  $K = 20$ .

Datasets	standard			
	<i>elbo</i>	<i>recons</i>	<i>kl</i>	<i>kl<sub>z x</sub></i>
StaticMNIST	-81.06	-69.02	<b>12.03</b>	1.59
MNIST	-79.88	-68.73	<b>11.15</b>	1.24
FashionMNIST	-225.60	-214.15	<b>11.45</b>	1.38
Omniglot	-91.58	-82.80	8.78	1.75
Datasets	RNVP $q(z x)$			
	<i>elbo</i>	<i>recons</i>	<i>kl</i>	<i>kl<sub>z x</sub></i>
StaticMNIST	-80.65	-67.91	12.75	<b>1.57</b>
MNIST	-79.59	-68.17	11.42	1.18
FashionMNIST	-225.05	-213.41	11.64	<b>1.24</b>
Omniglot	<b>-91.26</b>	-83.17	<b>8.10</b>	<b>1.57</b>
Datasets	RNVP $p(z)$			
	<i>elbo</i>	<i>recons</i>	<i>kl</i>	<i>kl<sub>z x</sub></i>
StaticMNIST	<b>-80.60</b>	<b>-62.22</b>	18.38	1.68
MNIST	<b>-79.28</b>	<b>-64.41</b>	14.87	<b>1.13</b>
FashionMNIST	<b>-224.65</b>	<b>-210.16</b>	14.49	1.26
Omniglot	-91.78	<b>-79.70</b>	12.07	2.16

## B.9 Additional results: learned prior on low posterior samples

Rosca et al. [28] proposed an algorithm to obtain *low posterior samples* ( $\mathbf{z}$  samples which have low likelihoods on  $q_\phi(\mathbf{z})$ ) from a trained VAE, and plotted the histograms of  $\log p_\lambda(\mathbf{z})$  evaluated on these  $\mathbf{z}$  samples. Their algorithm first samples a large number of  $\mathbf{z}$  from the prior  $p_\lambda(\mathbf{z})$ , then uses Monte Carlo estimator to evaluate  $q_\phi(\mathbf{z})$  on these  $\mathbf{z}$  samples, and finally chooses a certain number of  $\mathbf{z}$  with the lowest  $q_\phi(\mathbf{z})$  likelihoods as the *low posterior samples*. They also sampled one  $\mathbf{x}$  from  $p_\theta(\mathbf{x}|\mathbf{z})$  for each low posterior sample  $\mathbf{z}$ , plotted the sample means of these  $\mathbf{x}$  and the histograms of ELBO on these  $\mathbf{x}$ . Although we have found their Monte Carlo estimator for  $D_{KL}[q_\phi(\mathbf{z})||p_\lambda(\mathbf{z})]$  vulnerable (see

Appendix B.5), their *low posterior samples* algorithm only ranks  $q_\phi(\mathbf{z})$  for each  $\mathbf{z}$ , and the visual results of their algorithm seems plausible. Thus we think this algorithm should be still convincing enough, and we also use it to obtain *low posterior samples*.

To compare the learned prior with unit Gaussian prior on such *low posterior samples*, we first train a ResnetVAE with unit Gaussian prior (denoted as *standard ResnetVAE*), and then add a *post-hoc trained* RNVP prior upon this original ResnetVAE (denoted as *post-hoc trained ResnetVAE*). We then obtain 10,000  $\mathbf{z}$  samples from the *standard ResnetVAE*, and choose 100  $\mathbf{z}$  with the lowest  $q_\phi(\mathbf{z})$  among these 10,000 samples, evaluated on *standard ResnetVAE*. Fixing these 100  $\mathbf{z}$  samples, we plot the histograms of  $\log p_\lambda(\mathbf{z})$  w.r.t. *standard ResnetVAE* and *post-hoc trained ResnetVAE*. We also obtain one  $\mathbf{x}$  sample from  $p_\theta(\mathbf{x}|\mathbf{z})$  for each  $\mathbf{z}$ , and plot the histograms of ELBO for each  $\mathbf{x}$  (w.r.t. the two models) and their sample means. See Fig. B.4.

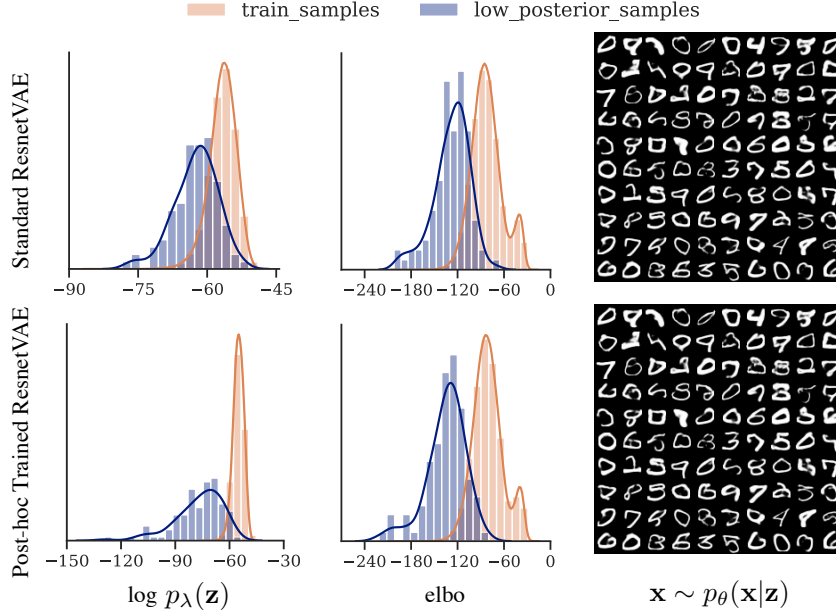


Figure B.4: (left) Histograms of  $\log p_\lambda(\mathbf{z})$  of the low posterior samples, (middle) histograms of ELBO of  $\mathbf{x}$  samples corresponding to each low posterior sample, and (right) the means of these  $\mathbf{x}$ , on *standard ResnetVAE* and *post-hoc trained ResnetVAE*.

The  $\mathbf{x}$  samples of *post-hoc trained ResnetVAE* (bottom right) are the same as those of *standard ResnetVAE* (top right), since *post-hoc trained ResnetVAE* has exactly the same  $p_\theta(\mathbf{x}|\mathbf{z})$  and  $q_\phi(\mathbf{z}|\mathbf{x})$  as *standard ResnetVAE*. However, the *post-hoc trained* prior successfully assigns much lower  $\log p_\lambda(\mathbf{z})$  (bottom left) than unit Gaussian prior (top left) on the *low posterior samples*, which suggests that a *post-hoc trained* prior can avoid granting high likelihoods to these samples in the latent space. Note *post-hoc trained ResnetVAE* also assigns slightly lower ELBO (bottom middle) than *standard ResnetVAE* (top middle) to  $\mathbf{x}$  samples corresponding to these *low posterior samples*.

To verify whether a learned prior can avoid obtaining *low posterior samples* in the first place, we obtained *low posterior samples* from a ResnetVAE with *jointly trained* prior (denoted as *jointly trained ResnetVAE*), see Fig. B.5. Compared to Fig. B.4, we can see that  $\log p_\lambda(\mathbf{z})$  of these *low posterior samples* and ELBO of the corresponding  $\mathbf{x}$  samples are indeed substantially higher than those of *standard ResnetVAE* and *post-hoc trained ResnetVAE*. However, the visual quality is not perfect, indicating there is still room for improvement.

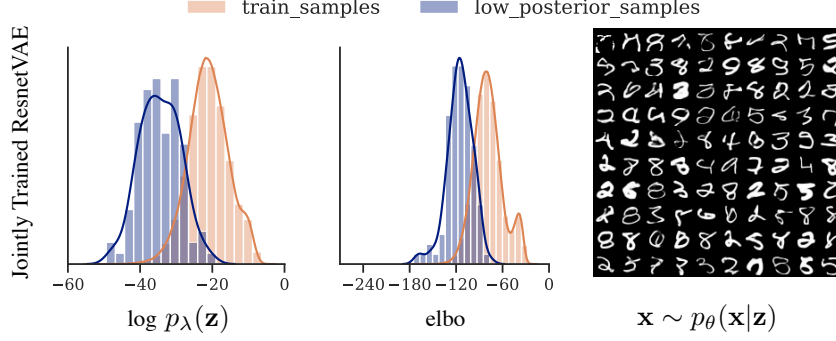


Figure B.5: (left) Histograms of  $\log p_{\lambda}(\mathbf{z})$  of the low posterior samples, (middle) histograms of ELBO of  $\mathbf{x}$  samples corresponding to each low posterior sample, and (right) the means of these  $\mathbf{x}$ , on *jointly trained* ResnetVAE.

### B.10 Wall-clock times

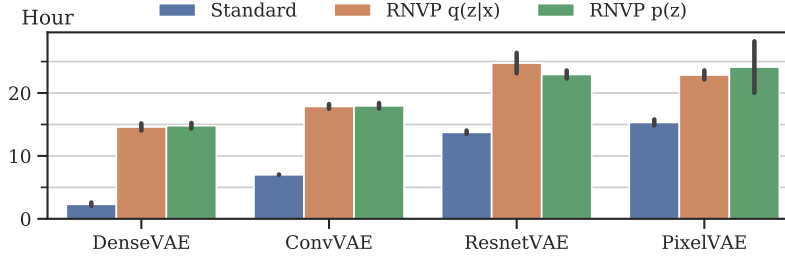


Figure B.6: Average training time of various models on MNIST, flow depth  $K = 20$ . Black sticks are standard deviation bars. For PixelVAE, training mostly terminates in half way due to early-stopping.

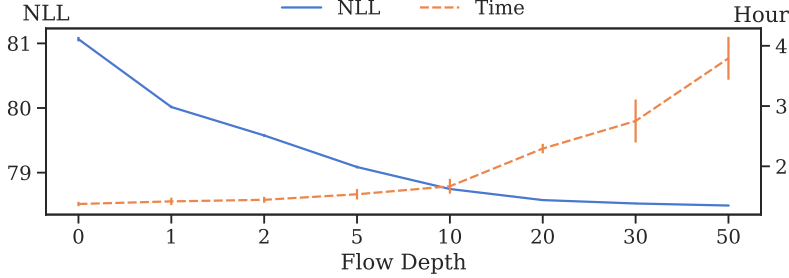


Figure B.7: Average training time and test negative log-likelihood (NLL) of ResnetVAE with RNVP prior of different flow depth. Vertical sticks are standard deviation bars.

We report the average training time of various models trained on MNIST, see Figs. B.6 and B.7. Each experiment runs on one GTX 1080 Ti graphical card. In Fig. B.6, we can see that the computational cost of RNVP prior is independent with the model architecture. For complicated architectures like ResnetVAE and PixelVAE, the cost of adding a RNVP prior is fairly acceptable, since it can bring large improvement. In Fig. B.7, we can see that for  $K > 50$ , there is likely to be little gain in test NLL, but the computation time will grow even larger. That's why we do not try larger  $K$  in our experiments.